



Engineering a cell-hydrogel-fibre composite to mimic the structure and function of the tendon synovial sheath



Angela Imere^{a,b}, Cosimo Ligorio^{a,c}, Marie O'Brien^{a,b}, Jason K.F. Wong^{d,e}, Marco Domingos^{b,f}, Sarah H. Cartmell^{a,b,*}

^a Department of Materials, School of Natural Sciences, Faculty of Science and Engineering, The University of Manchester, Manchester, UK.

^b The Henry Royce Institute, Royce Hub Building, The University of Manchester, Manchester, UK.

^c Manchester Institute of Biotechnology (MIB), The University of Manchester, Manchester, UK.

^d Blond McIndoe Laboratories, Division of Cell Matrix Biology & Regenerative Medicine, School of Biological Sciences, Faculty of Biology, Medicine and Health, The University of Manchester, Manchester, UK.

^e Department of Plastic Surgery & Burns, Wythenshawe Hospital, Manchester University NHS Foundation Trust, Manchester Academic Health Science Centre, Manchester, UK.

^f Department of Mechanical, Aerospace and Civil Engineering, School of Engineering, Faculty of Science and Engineering, The University of Manchester, Manchester, UK.

ARTICLE INFO

Article history:

Received 10 June 2020

Revised 5 November 2020

Accepted 10 November 2020

Available online 13 November 2020

Keywords:

Tendon synovial sheath

Anti-adhesion

Hyaluronic acid

Peptide hydrogel

Polycaprolactone

ABSTRACT

The repair of tendon injuries is often compromised by post-operative peritendinous adhesions. Placing a physical barrier at the interface between the tendon and the surrounding tissue could potentially solve this problem by reducing adhesion formation. At present, no such system is available for routine use in clinical practice. Here, we propose the development of a bilayer membrane combining a nanofibrous poly(ϵ -caprolactone) (PCL) electrospun mesh with a layer of self-assembling peptide hydrogel (SAPH) laden with type-B synoviocytes. This bilayer membrane would act as an anti-adhesion system capable of restoring tendon lubrication, while assisting with synovial sheath regeneration. The PCL mesh showed adequate mechanical properties (Young's modulus=19±4 MPa, ultimate tensile stress=9.6±1.7 MPa, failure load=0.5±0.1 N), indicating that the membrane is easy to handle and capable to withstand the frictional forces generated on the tendon's surface during movement (~0.3 N). Morphological analysis confirmed the generation of a mesh with nanosized PCL fibres and small pores (< 3 μ m), which prevented fibroblast infiltration to impede extrinsic healing but still allowing diffusion of nutrients and waste. Rheological tests showed that incorporation of SAPH layer allows good lubrication properties when the membrane is articulated against porcine tendon or hypodermis, suggesting that restoration of tendon gliding is possible upon implantation. Moreover, viability and metabolic activity tests indicated that the SAPH was conducive to rabbit synoviocyte growth and proliferation over 28 days of 3D culture, sustaining cell production of specific matrix components, particularly hyaluronic acid. Synoviocyte-laden peptide hydrogel promoted a sustained endogenous production of hyaluronic acid, providing an anti-friction layer that potentially restores the tendon gliding environment.

Crown Copyright © 2020 Published by Elsevier Ltd on behalf of Acta Materialia Inc.
This is an open access article under the CC BY license (<http://creativecommons.org/licenses/by/4.0/>)

Statement of significance

Post-operative tendon adhesions represent one of the most common complications in tendon surgery. Current treatments relying on inert physical barriers to obstacle adhesion formation lack bioactive cues to aid regeneration and restore

tendon function. In this study, we engineered a biologically active bilayer biomembrane by incorporating a synoviocyte-laden peptide hydrogel into a polymeric electrospun mesh. Our work clearly shows that the polymeric mesh acts as a physical barrier to adhesion-forming cells, while the peptide hydrogel layer provides anti-friction properties and supports 3D synoviocyte culture. In particular, encapsulated cells have the potential to restore tendon gliding performance and function in the long term *via* hyaluronic acid production. There-

* Corresponding author: Phone: +44 161 306 3567

E-mail address: sarah.cartmell@manchester.ac.uk (S.H. Cartmell).

fore, this cell-hydrogel-fibre composite harbours significant potential as a clinical tool for the treatment of tendon post-operative adhesions.

1. Introduction

Poor recovery from flexor tendon injury can lead to pain and disability, which in turn significantly impact upon an individual's global hand function, ability to work and confidence to contribute to society [1]. Currently, the gold standard for the management of flexor tendon injuries is based on strong suture repair methods and early-active hand therapy [2]. Although tenorrhaphy and mobilisation allow to re-join severed tendons and facilitate tissue healing, around 28% of cases present with poor restoration of function secondary to adhesions [3,4]. To date, several methods have been adopted for the treatment of adhesions, including various post-operative rehabilitation regimes, less invasive suture configurations and pharmacological adjuvants [5]. Moreover, recent studies have focused on investigating the inflammatory cascade involved in the process of adhesion formation, in order to obtain novel insights that could help to identify therapeutic targets to achieve scar-free tendon repair. For example, prostaglandin E2 through EP4, one of its downstream receptors [6], and the plasminogen activator inhibitor 1 (PAI-1/Serpine1) have been shown to play a regulatory role in tendon healing [7]. However, little consensus exists on the important factors for generating the best outcomes as, despite optimised care, patients can still present with poor function [8,9].

Injury to the flexor tendon results in disruption of the synovial sheath, whose main functions in physiological conditions are to create a protective membrane, minimise friction and lubricate tendon movement against a bone or a fibrous tissue [10]. To accomplish its functions, the parietal layer of synovial sheath acts as a biological barrier, while the visceral layer secretes the synovial fluid, an important extrinsic source of nutrition rich in hyaluronic acid (HA) [10]. HA, which is produced by type-B synoviocytes populating the synovial sheath [11], plays a key role in ensuring overall tendon gliding, while promoting nutrition to the process of intrinsic tendon healing in injured tendons [12].

In order to recreate a smooth surface after tendon injury without interfering with tendon healing and cell activity, biocompatible and permeable membranes could be used. Several barriers have been developed using poly(tetrafluoroethylene), HA, hydroxyapatite, bovine pericardium, as well as poly(vinyl alcohol) hydrogel [5,13]. However, they lack evidence on their gliding performance, which is the primary determinant of function in the long term, after completion of the tendon reparative phase (6–8 weeks) [14,15]. Moreover, only preclinical data is available on these barriers and too limited to support their clinical use [16]. Although strategies for adhesion prevention are limited for tendon, there are various options based on synthetic and natural polymeric membranes (e.g. Preclude®, Seprafilm®, SurgiWrap™, Intercceed®), as well as injectable hydrogels predominantly exploiting HA-based compounds (e.g. Hyalobarrier® and Intergel®) [17,18]. Randomised control studies have shown their efficacy for small-bowel surgery [19], colorectal [20] and gynaecologic [21,22] laparoscopy and open reconstructive pelvic surgery [23]. However, their use for tendon applications is limited due to short life-time *in vivo* [17], limited nutrient function at nearly avascular injury sites such as tendons [24] and failure to restore the architecture of tendon synovial sheath, thus leading to loss of barrier function.

In order to recapitulate the synovial membrane for prevention of adhesions on intrasynovial tendons, electrospinning technique is considered a good candidate [25]. Indeed, electrospin-

ning allows for manufacturing of fibrous membranes with tunable porosity, fibre dimension (from nano- to micro-scale) and pore size [26]. These are key parameters to prevent fibroblast migration from surrounding tissues and ensure transport of nutrients and waste. Several nanofibrous membranes for prevention of post-operative peritendinous adhesions have been prepared using different synthetic polymers, including poly(ϵ -caprolactone) (PCL) [25], poly(ethylene glycol)/PCL [27] and celecoxib-loaded poly(L-lactic acid)/poly(ethylene glycol) [28], all showing good barrier function against adhesion formation.

In order to ensure restoration of tendon glide, electrospun meshes can be coupled with hydrogels [25,28], where irregular friction surfaces are anticipated. Their high water content provides low-friction properties and injectability contributes to facilitate application [29]. Among the various classes of hydrogels, self-assembling peptide hydrogels (SAPHs) have recently attracted significant attention as they provide a water-rich (> 90%) self-supporting matrix that closely mimics the natural extracellular matrix (ECM), while offering immunocompatibility, biodegradability, tunable mechanical and structural properties and ease of handling [30]. Moreover, they are entirely synthetic, making them more reproducible and less immunogenic than their naturally-derived counterparts [31]. Among them, the class of β -sheet forming peptide hydrogels has been shown to exhibit shear-thinning properties that make them suitable for minimally invasive cell therapies [32]. In addition, their structure allows for ease of functionalisation by exploiting their molecular design [33].

Although SAPHs could potentially help tendon gliding in the first stages of tissue healing, they quickly degrade *in vivo* [34], thus being poorly efficient for long-term lubrication. For this reason, incorporating a source of endogenous production of HA (type-B synoviocytes) could offer an avenue to create a *de novo* matrix, which is fundamental to aid the regeneration of the synovial sheath and ensure low-friction properties also in late stages of tendon healing [35].

The aim of this study is to develop a bilayer biomembrane to be wrapped around the injured tendon with the potential to hinder post-operative adhesions, restore tendon gliding ability and support synovial sheath repair, as illustrated in Fig. 1. We hypothesised that an electrospun nanofibrous PCL mesh placed externally could provide mechanical stability to the biomembrane, while impeding infiltration of adhesion-forming cells. On the other side, a hydrogel layer based on a commercial β -sheet forming SAPH, Alpha4 from Manchester Biogel (UK), placed in contact with the tendon surface could facilitate smooth tendon motion in the early stages of tendon healing, while creating an ECM-like environment for encapsulated type-B synoviocytes. The latter are expected to secrete HA and provide bioactivity to the membrane for long-term lubrication purposes. To the best of authors' knowledge, this is the first time that Alpha4 was used as a 3D scaffold for the culture of synoviocytes. In this approach, the incorporation of a synoviocyte-laden hydrogel into a physical barrier represents a unique added value to the design of this biomembrane.

2. Materials and Methods

2.1. Fabrication of PCL electrospun mesh

PCL in the form of pellets ($M_n=50,000$) was purchased from Perstorp (UK) and used to generate electrospun polymeric meshes. Initially, a 10% (w/v) PCL solution was prepared by dissolving PCL pellets in 1,1,1,3,3,3-hexafluoro-2-propanol (Sigma Aldrich, UK) overnight at room temperature. Afterwards, employing a Spray-base® electrospinning system (Profactor Life Sciences, Ireland) equipped with a 18 G needle and flat collector, and setting the process parameters at 1 ml/h flow rate, 20 kV high voltage, 20 cm

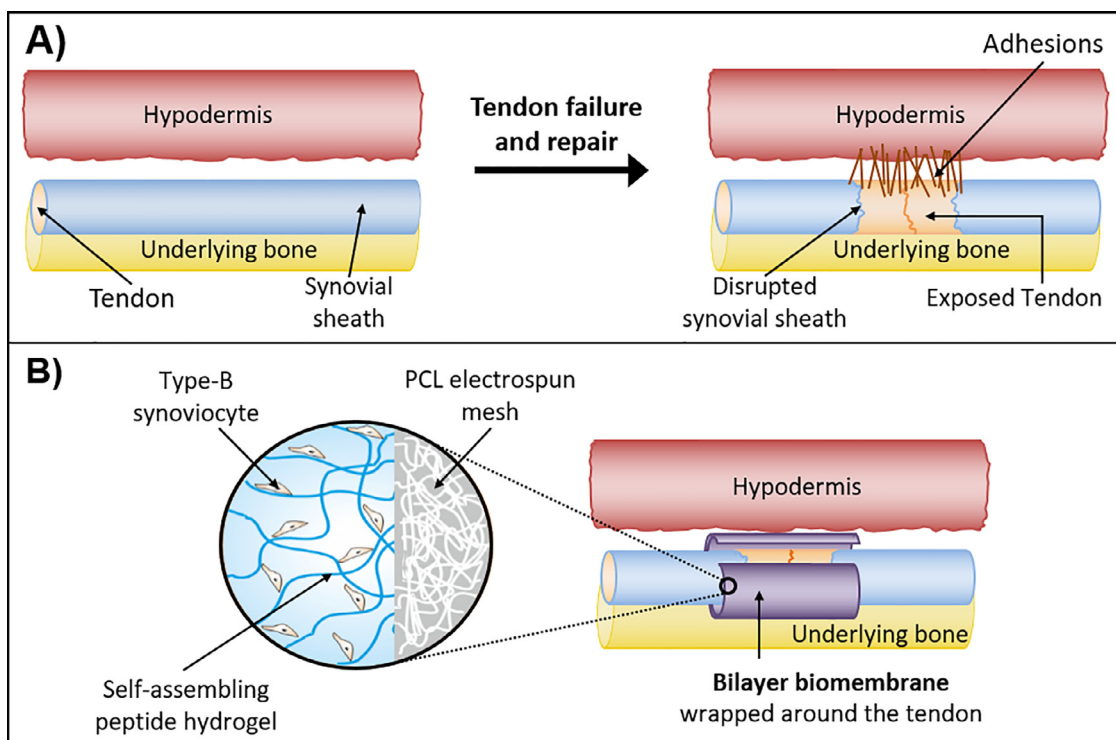


Fig. 1. Overview of bilayer biomembrane for prevention of post-operative tendon adhesions. **A)** Schematic of native synovial sheath around the tendon (left) and disruption of tendon synovial sheath upon tendon failure and repair, which leads to the formation of adhesions between the exposed tendon and hypodermis (right). **B)** Schematic of proposed approach to impede adhesion formations. A bilayer biomembrane is wrapped around the tendon. This bilayer biomembrane is formed by an external PCL electrospun mesh that acts as a physical barrier to stop the infiltration of adhesion-forming cells and provides mechanical stability to the biomembrane for ease of use. The second layer, in contact with the tendon, is a SAPH that ensures early-stage lubrication and provides an ECM-like environment for encapsulated type-B synoviocytes. These cells produce HA and are responsible for tendon long-term lubrication.

needle-collector distance and 1 h spinning time, it was possible to obtain electrospun PCL meshes. Finally, the meshes were removed from the collector and dried under vacuum for 24 h before further characterisation in order to allow complete evaporation of solvent residues.

2.2. Morphological characterisation of PCL mesh

PCL meshes were mounted on standard Scanning Electron Microscopy (SEM) pin stubs using conductive double-sided adhesive carbon tabs, sputter coated with Gold-Palladium (3 nm-thick coating) and imaged with a Hitachi S-3000N SEM. Fibre diameters were analysed using ImageJ (v.1.53e) and fibre distributions were obtained from a minimum of 300 fibres.

Pore size was obtained using ImageJ (v.1.53e) by segmenting the SEM images with the IsoData thresholding technique. Using the “analysing particle” tool, pore areas were recorded and converted into equivalent pore diameter.

The apparent porosity (P_{app}) of the PCL mesh ($n=6$) was obtained, as previously described, using the following equation:

$$P_{app} (\%) = \left(1 - \frac{M}{\rho V}\right) \times 100 \quad (1)$$

where M is the mass of the fibrous mesh, ρ is the PCL density (1.145 g cm^{-3}), and V is the volume of the mesh [36].

2.3. Mechanical characterisation of PCL mesh

Mechanical tests were performed based on previous works [37,38]. Samples ($n=8$) were prepared by cutting strips of PCL mesh (width: 5 mm, length: 57 mm) that were mounted on cardboard windows (window width: 10 mm, window length: 25 mm)

with double-sided tape. Mounted windows were gripped within the tensile grips and the cardboard sides cut. Tensile tests were performed in dry conditions using an Instron 3344 equipped with a 10 N load cell at strain rate of 5 mm/min. Cross-sectional area was assumed to be rectangular and was determined by multiplying the sample width by the thickness. Load, displacement, stress and strain data was collected and analysed to obtain Young's modulus, ultimate tensile stress, strain at failure and failure load. The Young's modulus was obtained as the slope of the stress-strain curve in the elastic linear region, which was determined by a linear fit having $R^2 > 0.98$. The ultimate tensile stress was evaluated as the maximum stress experienced by the meshes, while the strain and load at the breaking point were used as strain and load at failure respectively.

2.4. Migration study

3T3 cells (mammalian fibroblast line) were cultured in Dulbecco's Modified Eagle's medium (DMEM) supplemented with 10% heat-inactivated Foetal Bovine Serum (FBS) and 1% Antibiotic/Antimycotic (A/A) solution. All supplies were purchased from Sigma Aldrich (UK). Fibroblast migration was estimated using a double chamber system ($n=3$ per condition), as illustrated in Fig. 3A. PCL meshes were mounted onto 24-well inserts (Grenier Bio-One, UK) after removal of the insert membrane using the Dow-Corning 732 Silicone Sealant and sterilised by exposing to 70% ethanol and UV-light for 1 h. Insert membranes ($8 \mu\text{m}$ pore diameter) were used as negative control. Meshes were pre-conditioned in serum-free medium for 2 h at 37°C and 5% CO_2 and then media was removed prior to cell culture. Cells were seeded at passage 4 onto the upper chamber at 0.5×10^5 cells per well using serum-free DMEM and allowed to migrate to the lower chamber (containing

10% FBS DMEM) for 24 h at 37°C and 5% CO₂. Following incubation, cell migration was evaluated using immunofluorescence and AlamarBlue assay.

For AlamarBlue assay, migrated cells were detached by adding trypsin to the receiver well. After deactivation with 10% FBS media, cells were exposed to 10% AlamarBlue in DMEM for 4 h at 37°C and 5% CO₂. Following incubation, the solution was transferred to a 96-well plate (200 µl per well in triplicates) and fluorescence intensity measured using FLUOstar OPTIMA plate reader (excitation wavelength: 530 nm; emission wavelength: 590 nm). The measured fluorescence intensity was normalised to the fluorescence intensity of blanks (acellular AlamarBlue working solution in well) subtracting the average fluorescence intensity of blanks to each value.

To confirm outcomes from AlamarBlue assay, immunofluorescence staining was performed on migrated cells after 24 h of incubation. Non-migrated cells were removed from the upper chamber using a cotton swab. Inserts were then fixed in 10% neutral buffered formalin (NBF) for 30 min. Samples were permeabilised for 5 min with a 0.2 M glycine and 0.5% Triton-X-100 permeabilising solution and exposed for 30 min to 2% fish skin gelatin (FSG) (Sigma Aldrich, UK). Finally, samples were stained for F-actin and nuclei using Alexa Fluor 488® phalloidin (1:40 dilution in 2% FSG) and DAPI (1:1000 dilution in 2% FSG) respectively. After mounting with Prolong Diamond Antifade, samples were imaged using CQ1 confocal microscope (Yokogawa, Japan).

2.5. Characterisation of Alpha4 SAPH

2.5.1. Attenuated total reflectance Fourier-transform infrared spectroscopy (ATR-FTIR)

Secondary structure of Alpha4 SAPH (Manchester BIOGEL, UK) was investigated with ATR-FTIR. Measurements were performed on a Thermo-Fisher Nicolet 5700 FTIR spectrophotometer equipped with an attenuated total reflectance (ATR) diamond accessory. 20 µl of hydrogel was pipetted onto the crystal surface of the spectrophotometer and the beam path purged with dry CO₂-scrubbed air. Absorbance spectra were obtained using the average of 128 scans with a 4 cm⁻¹ resolution. High pressure liquid chromatography grade water background was subtracted from each spectra using the built-in OMNIC software provided with the instrument. All measurements were performed in triplicates. The FTIR spectra were smoothed using a Savitzky-Golay filter with a 9-points window. A baseline was subtracted in the Amide I region (1500–1700 cm⁻¹) from the original spectra using OriginPro 2017 software.

2.5.2. Atomic force microscopy (AFM)

Alpha4 hydrogel was first diluted 20-fold using double distilled water (ddH₂O). 50 µl of diluted hydrogel were then drop-cast on freshly cleaved mica and left to adhere for 2 min. Excess solution was then removed from the surface of the specimens and the mica stubs rinsed 10-times by pipetting 100 µl of ddH₂O directly onto the surface. Excess liquid was finally removed using Whatman No. 1 filter paper. Samples were left to air-dry overnight before imaging. AFM imaging was performed on a Bruker Multimode 8 instrument (Bruker, USA). Samples were scanned in air at room temperature in ScanAsyst mode, using a ScanAsyst-Air probe with a resonant frequency of 70 kHz and a nominal spring constant of 0.4 N m⁻¹. AFM images were acquired at a 512×512 pixels resolution over scanning areas ranging from 1.5×1.5 µm to 5×5 µm at a scan frequency of 1 Hz and analysed with Nanoscope Analysis 1.40 software. Fibre height distribution was obtained from approximately 100 fibres.

2.5.3. Oscillatory shear rheology

Rheological properties of acellular and cellular Alpha4 hydrogel were investigated using a Discovery Hybrid 2 (DHR-2) rheometer (TA Instruments, USA) using a 20 mm parallel plate geometry with a gap size of 500 µm (axial force at equilibrium ~0.05 N). For acellular hydrogels, “dry” samples were tested as formulated pipetting 200 µl of Alpha4 hydrogel onto the bottom rheometer plate. Acellular media-conditioned samples were prepared by pipetting 200 µl of Alpha4 hydrogel into 24-well inserts (1 µm pore size Greiner Bio-One, UK). The inserts were then placed into 24-well plates and incubated at 37°C and 5% CO₂ overnight in synoviocyte culture media (see Section 2.7). Cellular samples (200 µl) were tested at day 1 and 28 after culture and prepared as described in Section 2.7. After media exposure (acellular hydrogels) or designated culture time (cellular hydrogels), samples were removed from the inserts and transferred onto the rheometer plate. Then, the upper rheometer head was lowered to the desired gap size and samples were left to equilibrate for 3 min at 37°C. Amplitude sweep experiments were performed at 1 Hz frequency in the oscillation strain range of 0.01–100%. Frequency sweep experiments were performed at 0.2% strain, within the linear viscoelastic region (LVR) in the frequency range of 0.01–10 Hz. For recovery experiments, samples were tested in time-sweep mode by alternating cycles of low shear (300 s at 0.2% strain and 1 Hz frequency) with cycles of high shear (300 s at 100% strain and 1 Hz frequency). Flow sweep experiments were performed in the shear rate range of 1–1000 s⁻¹. All measurements were performed in triplicates (n=3) to ensure reproducibility.

2.5.4. Evaluation of anti-friction properties of the bilayer biomembrane

Characterisation of the bilayer membrane anti-friction properties was performed by oscillatory shear rheometric measurements using a Discovery Hybrid 2 (DHR-2) rheometer (TA Instruments, USA) using a 20 mm parallel plate geometry. Gap size was adjusted for each measurement in order to maintain a constant axial force of ~0.05 N at equilibrium. Tendon, hypodermis and synovial sheath samples were dissected from the central two toes of fresh porcine forelimb trotters and stored in Dulbecco's Phosphate-buffered saline (D-PBS) to maintain tissue hydration. Tissue samples were tested on the day of dissection within 8 h of slaughter. Four different samples were tested: porcine synovial sheath was used as positive control; gel only was used to determine the failure mode; PCL electrospun mesh with Alpha4 hydrogel – named ‘Membrane (Gel)’ – was used as test; PCL mesh with Dow-Corning 732 Silicone glue – named ‘Membrane (Glue)’ was used as negative control. These samples were mounted on the upper rheometer head (Fig. 6A i-iii). When tendon or hypodermis were used as contact surface, the tissues were fixed to the rheometer bottom plate (Fig. 6A iv-vi).

Once samples were loaded on the rheometer, the upper rheometer head was lowered to the desired gap size and samples were left to equilibrate for 3 min at 37 °C. Stress ramp experiments were performed in linear mode in the shear stress range of 0–300 Pa at a rate of 1.5 Pa s⁻¹. All measurements were repeated in triplicates (n=3) to ensure reproducibility. Yield stress values were obtained as the shear stress at peak viscosity observed in the stress ramp. For samples containing glue, no peak viscosity was observed, therefore, in order to compare with other samples, the yield stress value was obtained as the shear stress at maximum viscosity.

2.6. Synoviocyte cell culture and encapsulation

HIG-82 cells (rabbit synoviocytes, ATCC® CRL-1832™) were cultured in Ham's F12 medium (Lonza, Switzerland) supplemented with 10% non heat-inactivated FBS (Sigma Aldrich, UK) and 1% A/A.

In order to prepare cells for encapsulation, after trypsinisation and counting, a cell suspension containing the required number of cells was centrifuged to obtain a cell pellet. Supernatant medium was removed and cell pellet re-suspended in media at a concentration of 4×10^7 cells/ml of media. Cells up to passage 5 were encapsulated in Alpha4 hydrogel by gently mixing the cell suspension in the gel to obtain a final concentration of 4×10^6 cells/ml of gel. After encapsulation, 100 μ l of cell-laden gel was pipetted into 24-well inserts (1 μ m pore membrane), which were then placed into a 24-well culture plate. Culture media (800 μ l) was added into the lower chamber and cell-laden gel was left to settle for 5 min before adding 200 μ l of media onto the sample in the upper chamber. After preparation, samples were incubated at 37°C and 5% CO₂ and media was changed twice in the first hour without disturbing the hydrogel in order to neutralise gel's pH. After the first day, media was replaced every other day for the entire culture period.

2.7. Assessment of synoviocyte viability

Cell viability was assessed after 1, 3, 7, 14, 21 and 28 days from encapsulation by LIVE/DEAD assay (Life Technologies Ltd., UK) (n=3 per time point). The working solution was prepared by adding 1 μ l of 2 μ M calcein AM and 4 μ l of 4 μ M EthD-1 in 2 ml of D-PBS. Before staining cell-laden gels, media was removed and samples were covered with 1 ml of working solution and incubated for 1 h at 37°C and 5% CO₂. After incubation, samples were washed with D-PBS, moved onto glass slides and squashed using glass coverslips for imaging. Fluorescence microscopy was used for observations using an Eclipse 50i fluorescence microscope (Nikon UK Ltd., UK) with 494 nm (green, calcein AM) and 535 nm (red, EthD-1) emission filters. Quantification of cell viability was performed as previously described [32]. Briefly, fluorescence composite images were split in red, green and blue channels using ImageJ (v.1.53e) to produce three 8-bit greyscale images. Greyscale images were subject to thresholding using Huang's method [39] and a watershed algorithm was applied to separate touching cells. Using the "analysing particle" plugin, the number of live and dead cells was obtained from the greyscale images of the green and red channel respectively. Percentage viability was calculated as $100 \times [\text{number of live cells}/\text{total number of cells}]$.

2.8. Assessment of synoviocyte metabolic activity

Cell metabolic activity and proliferation was assessed after 1, 3, 7, 14, 21 and 28 days from encapsulation by AlamarBlue assay (n=3 per time point). Media was gently removed and 10% AlamarBlue in Ham's F12 was added on upper and lower chamber. After 4 h of incubation at 37°C and 5% CO₂, the AlamarBlue solution was gently removed from the top chamber and mixed with the lower chamber solution. Then, the mixed solution was transferred to a 96-well plate (200 μ l per sample in triplicates) and fluorescence intensity was measured using FLUOstar OPTIMA plate reader (excitation wavelength: 530 nm; emission wavelength: 590 nm). The measured fluorescence intensity was normalised to the fluorescence intensity of blanks (hydrogels with no cells) subtracting the average fluorescence intensity of blanks to each value.

2.9. Histological evaluation of synoviocyte-laden hydrogel

Histological evaluation of synoviocyte-laden Alpha4 constructs was performed after 28 days of culture. Samples (n=3) were fixed in 10% NBF for 30 min and washed twice with D-PBS. Once fixed, hydrogels were processed overnight using a VIP 2000 (Vacuum Infiltration Processor, Miles Scientific, UK). Samples were embedded in paraplast paraffin wax (Sigma Aldrich, UK) and sectioned along the longitudinal plane using a Leica RM2145 microtome. Sample

were cut as 5 μ m-thick slices and deposited on SuperFrost™ glass slides (ThermoScientific, UK). Sections were de-waxed in xylene, followed by re-hydration in descending grades of ethanol to water. They were stained separately with haematoxylin and eosin (H&E), Gomori trichrome, Picrosirius Red (PSR) and Alcian Blue according to Scott Method, as previously described [35]. Acellular hydrogel constructs and human synovium tissue obtained from the knee of 2 patients were used as negative and positive controls, respectively.

Immunohistochemical evaluation of synoviocyte-laden Alpha4 constructs was performed after 28 days. Samples were initially processed as described above and deposited on SuperFrost™ Plus glass slides (ThermoScientific, UK). Sections were de-waxed in xylene for 5 min, followed by rinsing in descending grades of ethanol. Antigen retrieval was performed using EDTA pH9 and proteinase K buffers for HA and type-I collagen (incubation for 30 and 10 min respectively at 90°C and 37°C). Histological sections were blocked in 2.5% goat serum or horse serum (10 min at room temperature) followed by staining overnight at 4°C with anti-HA primary antibody (1:50 dilution, mouse monoclonal, product code: LS-C315053 (LS Biosciences, UK)) or anti-collagen I primary antibody (1:100 dilution, goat polyclonal, product code: 1310-10 (SouthernBiotech, US)). After removal of primary antibody, sections were treated with secondary antibody (1:200, biotinylated goat anti-mouse or horse anti-goat, 30 min at room temperature). Sections were then treated with avidin-biotin complex (Vector, UK) for 30 min at room temperature, washed in PBS for 5 min and then treated with DAB substrate (Vector, UK) for 5 min. Nuclear fast red was used for the counter-staining. Hydrogel constructs and human synovium tissue not exposed to a primary antibody were used as negative controls. Acellular constructs were also used as further negative controls to ensure no positive staining of the hydrogel, while human synovium tissue was used as positive control for direct comparison with cellular hydrogel. Validation of primary antibodies was performed on human synovium tissue (HA) and porcine skin (collagen I) (Fig. ESI 1).

All sections were de-hydrated in ascending grades of ethanol, cleared in xylene and coverslips applied using DPX mountant (Sigma Aldrich, UK). Samples were imaged using a LEICA DM2700M microscope.

2.10. Statistical analysis

All results were reported as mean \pm standard deviation (SD), unless otherwise stated. Statistical comparison between multiple groups was analysed by One-Way ANOVA with Tukey post-hoc test using OriginPro 2017 at 95%, 99% and 99.9% confidence levels.

2.11. Ethical consideration

Ethical approval for the use of human synovium tissue was obtained by the North West - Liverpool Central Research Ethics Committee through the Liverpool Musculoskeletal Biobank (15/NW/0661). The study was conducted in full conformance with principles of the "Declaration of Helsinki", Good Clinical Practice (GCP) and within the laws and regulations of the country in which the research was conducted. Informed consent was also obtained from all the patients involved in the study and confidentiality of clinical details and personal information of the patients was maintained.

3. Results and Discussion

3.1. Characterisation of PCL electrospun mesh

In this study, a bilayer biomembrane is proposed for the prevention of post-operative tendon adhesions and restoration of ten-

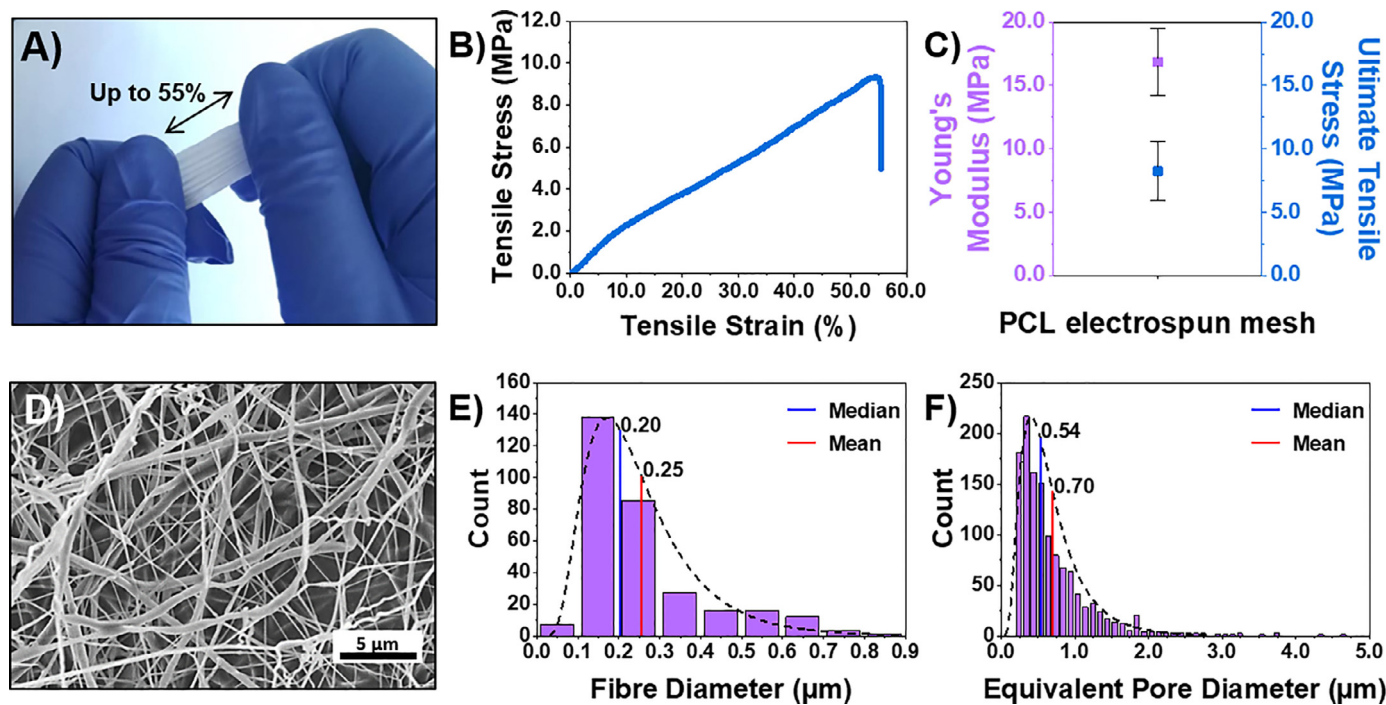


Fig. 2. Mechanical and morphological characterisation of PCL electrospun mesh. **A)** The PCL electrospun mesh can be stretched up to 55% without failure and shows ease to be handled. **B)** Representative stress-strain curve under tension, showing the predominantly elastic behaviour of the PCL mesh. **C)** Young's modulus and ultimate tensile stress ($n=8$; Data shown as mean \pm SD). **D)** SEM image, showing morphology of PCL mesh. **E)** Distribution of mesh fibre diameter. **F)** Distribution of equivalent pore diameter indicates the average dimension of the mesh pores.

don gliding ability. In view of use in a clinical setting, the product needs to be easily manoeuvrable and controllable by the surgeon [16]. Therefore, a PCL mesh was obtained using electrospinning process to create the structural support of the bilayer biomembrane. As demonstrated in Fig. 2A, the PCL mesh could be easily handled and stretched up to 55% its initial length without any visible tearing or major deformations by naked eye observation. Moreover, the PCL membrane shows a predominantly elastic behaviour under tension and limited plastic deformation (Fig. 2B), with a strain at failure of $55\pm 8\%$, indicating the ability of the product to be easily handled and anchored in place without the risk of breaking during implantation. Indeed, these mechanical behaviour is in accordance with the results obtained on similar nanofibrous PCL meshes that have been successfully implanted *in vivo* for tendon anti-adhesion applications [25,27].

The mechanical behaviour of the PCL electrospun membrane also plays a key role in determining the final biomembrane resistance to the frictional forces generated during tendon movement. Frictional forces arising from the movement of *flexor digitorum profundus* tendon relative to the sheath (A2 pulley) have been reported to range from 0.02 N to 0.31 N when a 4.9 N load is applied to the tendon [40]. In this study, the PCL electrospun mesh possesses high mechanical properties in terms of Young's modulus (19 ± 4 MPa) and ultimate tensile stress (9.6 ± 1.7 MPa) (Fig. 2C) and withstands a maximum load of 0.5 ± 0.1 N without breaking, as shown in Fig. ESI 2. Although these mechanical properties have been tested in dry conditions, it is expected that the changes due to a moist environment would still be appropriate, since wet conditions would determine only a slight decrease in stiffness, in favour of a drastic increase in strain at failure and consequently toughness, as previously reported [41]. Moreover, the hydrophobic nature of PCL reduces its degradation kinetics and helps maintaining mechanical resistance over time [42]. These results indicate that the mesh could provide mechanical stability to the proposed bilayer biomembrane, without failing during tendon move-

ment, since the mesh failure load (0.5 ± 0.1 N) is higher than the expected frictional forces (0.2–0.31 N). The membrane mechanical integrity is mainly required until completion of the tendon reparative phase, which has been reported to last for 6–8 weeks [14,15]. As described by Bölgen *et al.*, the molecular weight of PCL electrospun meshes upon subdermal implantation in a rat model decreases by 10% in the first 45 days, while a 27% drop is observed after 90 days [43]. Although the PCL degradation rate is highly affected by its shape and surface area-to-volume ratio, the literature suggests that the degradation profile of PCL electrospun membranes is slow enough to guarantee the appropriate mechanical integrity required for tendon healing [43].

In addition to mechanical stability, the PCL mesh was also conceived to act as a physical barrier to fibroblast migration to reduce tendon extrinsic healing. Indeed, recruitment and infiltration of fibroblasts from surrounding tissues during tendon healing was reported to contribute to the process of scarring and adhesion formation [44,45]. In order to effectively block cell infiltration, the barrier must possess a pore size that is small enough to impede cell migration, still ensuring nutrients and waste exchange. Previous studies have demonstrated that fibre diameter strongly affects pore size [46], which in turn determines cell behaviour in terms of adhesion, proliferation and infiltration [47–49]. In particular, it has been shown that larger fibres produce a smaller pore size as result of increased fibre packing density during the electrospinning process [47–49]. Analysis of SEM images (Fig. 2D–F) shows that the selected spinning parameters produce a homogeneous mesh with an average fibre diameter smaller than $0.3\ \mu\text{m}$ (Mean = $0.25\ \mu\text{m}$, Median = $0.20\ \mu\text{m}$). As expected, the nanofibrous PCL mesh exhibits a small equivalent pore size (Mean = $0.70\ \mu\text{m}$, Median = $0.54\ \mu\text{m}$), as shown in Fig. 2F, still maintaining a high apparent porosity ($P_{app} = 88.5\pm 1.1\%$) for nutrients, oxygen and waste exchange. Considering that the average dimension of fibroblast cells is $\sim 10\ \mu\text{m}$ ($50\ \mu\text{m}$ when cells spread out and flatten) [48], this value of pore size suggests that the mesh has the poten-

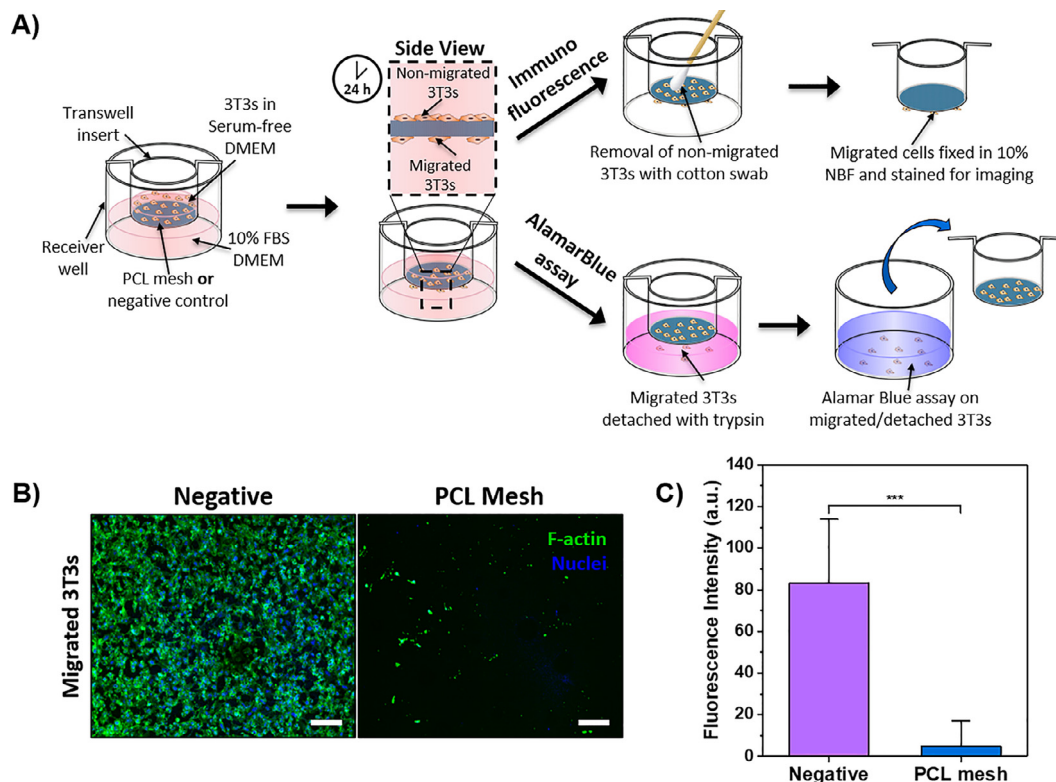


Fig. 3. Evaluation of fibroblast migration through the PCL electrospun mesh. **A)** Schematic of experimental set-up. Fibroblasts were seeded on the PCL mesh using a transwell insert and allowed to migrate for 24 h under the effect of a chemoattractant (a gradient of FBS). Samples ($n=3$ per condition) were analysed using two methods: immunofluorescence and AlamarBlue assay. For immunofluorescence, non-migrated cells lying on top of the membrane were removed with a cotton swab and migrated cells were fixed and stained for subsequent imaging. For AlamarBlue assay, trypsin was added to the receiver well to detach migrated fibroblasts only. Then, AlamarBlue assay was performed on trypsinised cells. **B)** Immunofluorescence of 3T3 cells migrated through the PCL mesh compared to negative control ($8\ \mu\text{m}$ pore insert membrane) shows minimal fibroblast migration. Migrated cells were stained for F-actin (green) and nuclei (blue). Scale bar = $100\ \mu\text{m}$. **C)** Alamar Blue assay performed on migrated and detached 3T3s confirms minimal migration of fibroblasts compared to negative control. (Data is shown as mean \pm SD; *** p -value < 0.001).

tial to stop the infiltration of adhesion-forming cells. Moreover, it has been reported that fibre morphology influences cell ability to bind across and align along individual fibres. If fibres are in the micrometre range, cells are able to align to fibres and closely interact with them [50], while if nanosized fibres are present, cells tend to distribute randomly on the scaffold and their infiltration is dampened as result of decreased pore size [50,51].

Although a small pore size is a theoretical indicator of the mesh capability to stop the infiltration of adhesion-forming cells, it is imperative to corroborate this hypothesis with experimental data. Confirmation that the PCL mesh acts as physical barrier was demonstrated by studying the ability of fibroblasts to migrate through the polymeric membrane under the effect of a serum concentration gradient (Fig. 3A). Immunofluorescence analysis (Fig. 3B) indicates that fibroblasts are not able to pass through the PCL mesh, although they migrate across a membrane with larger pores ($8\ \mu\text{m}$) used as negative control. The anti-adhesion and blocking effect of the PCL mesh was also validated by AlamarBlue assay, as reported in Fig. 3C. Other studies have evaluated the underlying mechanism of anti-adhesion effect of various membranes using similar *in vitro* experimental settings [24,25,27]. These authors showed that the ability of a membrane to stop the migration and infiltration of fibroblasts resulted also in reduced adhesions *in vivo* [24,25,27]. Therefore, we envisage that the PCL mesh can create a physical barrier not only *in vitro*, but that this action could be also replicated *in vivo*. Although the scope of this publication focuses on *in vitro* assessment of this new approach, future work will include corroborating this assumption by performing animal studies.

3.2. Characterisation of Alpha4 SAPH

While the PCL electrospun mesh has been shown to possess sufficient mechanical properties to facilitate biomembrane application and stability during and after surgery and to create a physical separation between the tendon and surrounding tissues, it does not provide any support towards recovery of tendon gliding ability. Therefore, a hydrogel was employed as an early-stage lubrication layer in the biomembrane in order to help tendon gliding in the early phases of tissue healing. Among all, synthetic peptide hydrogels were identified as suitable candidates due to their inherent tailorable properties that can support various cell types [52]. To the best of authors' knowledge, no other works have applied peptide-based hydrogels for synovial sheath regeneration. Therefore, after screening of four different SAPHs available in the market, Alpha4 was chosen as it was considered the most adequate for its intended use in terms of biocompatibility and viscoelastic properties (for details see Fig. ESI 3).

Alpha4 belongs to a class of hydrogels based on the bottom-up design of β -sheet forming peptides, which has been previously used in TE, with different cell types both as cell carriers [32,53,54] or drug delivery platforms [55–57]. Microstructural characterisation of Alpha4 hydrogel was performed using AFM and ATR-FTIR (Fig. 4). Alpha4 forms a uniform nanofibrous network (fibre height = $1.6 \pm 0.2\ \text{nm}$) that presents with characteristic intermediate structures typical of β -sheet forming peptides [58] (inset ii in Fig. 4A). To confirm that β -sheet rich nanofibres are formed in the hydrogel, ATR-FTIR spectra were recorded in the amide region ($1700\text{--}1500\ \text{cm}^{-1}$), as shown in Fig. 4 C. Data indicates a peak

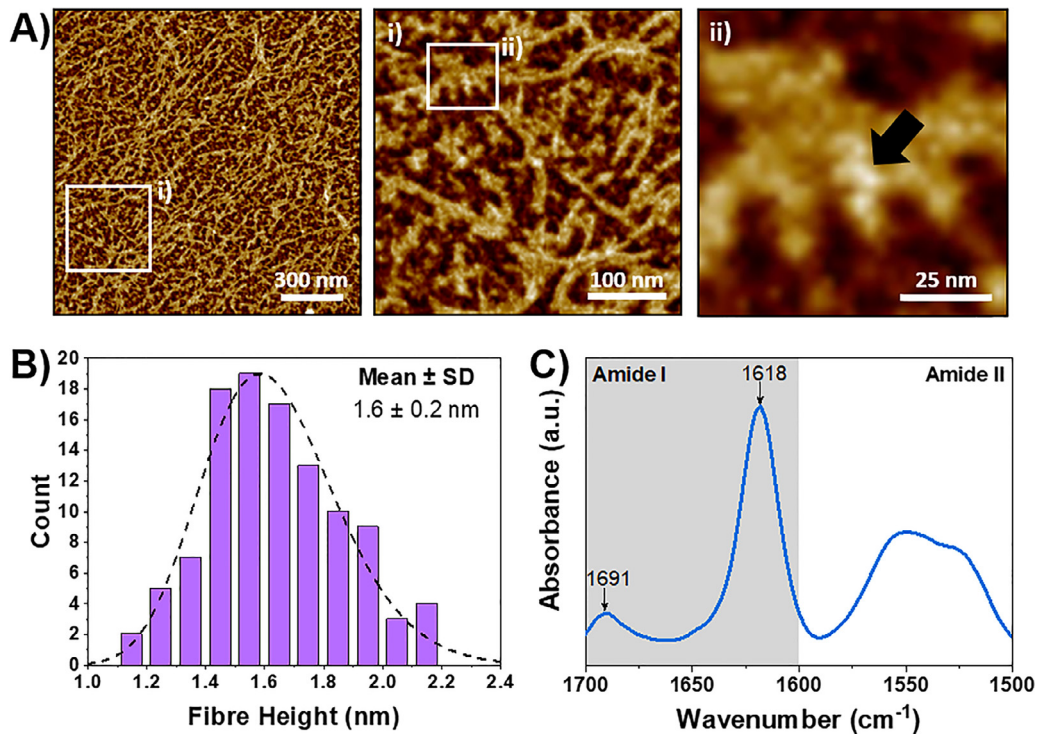


Fig. 4. Morphological characterisation of Alpha4 SAPH. A) AFM image of the hydrogel over a scan window of $1.5 \mu\text{m} \times 1.5 \mu\text{m}$ shows the hydrogel nanofibrillar network. Inset **i)** shows the fibrous network at higher magnification. Inset **ii)** shows a characteristic helical ribbon feature of β -sheet forming peptides (indicated by black arrow). B) Distribution of hydrogel's fibre height confirms the presence of nanofibres. C) ATR-FTIR shows two peaks in the Amide I region (grey area) that indicate the presence of antiparallel β -sheets.

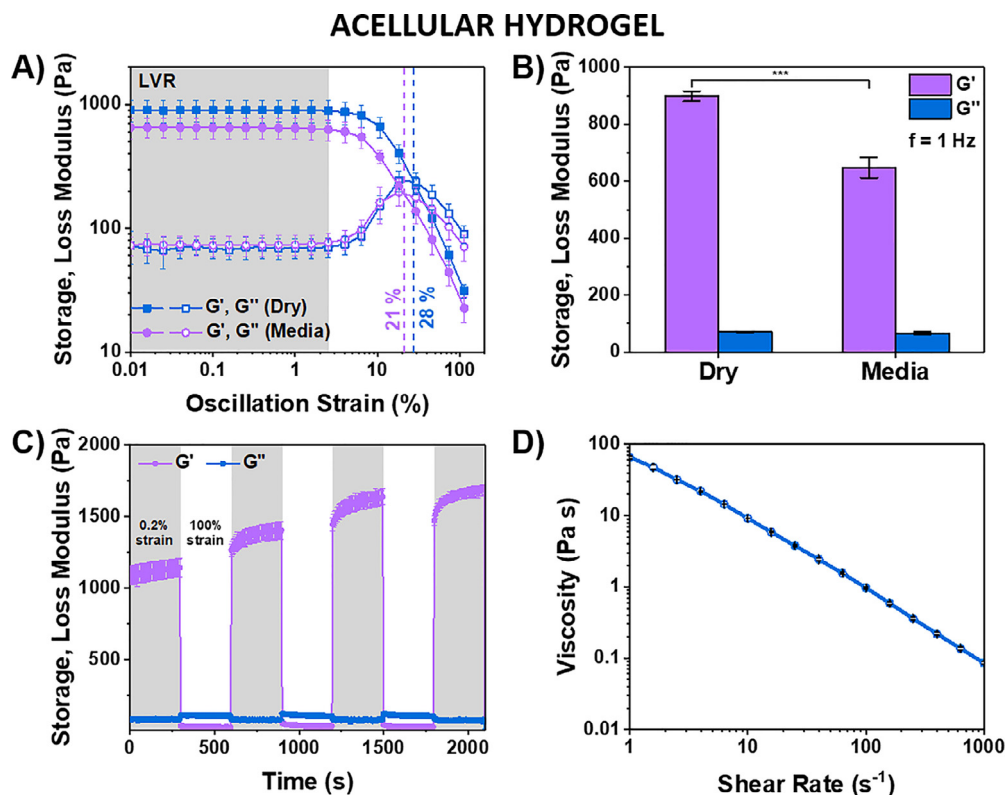


Fig. 5. Oscillatory shear rheology of acellular Alpha4 SAPH. A) Mechanical properties of the hydrogel were tested via amplitude sweep experiments performed before ('Dry') and after media conditioning ('Media'). Dry samples were tested as formulated, while media-conditioned sample were tested after overnight exposure of the hydrogel to Ham's F12 culture media. The grey area indicates the LVR region. B) Average values of storage and loss moduli of hydrogel at 1 Hz before and after media conditioning describe the network visco-elasticity properties of the hydrogel. C) Recovery experiments with low (0.2%, grey areas) and high (100%, white areas) strain deformation and D) flow sweep experiments show self-healing and shear-thinning properties of the hydrogel before media conditioning. All measurements were performed in triplicates ($n=3$) at 37°C . (Data is shown as mean \pm SD; $***p\text{-value} < 0.001$).

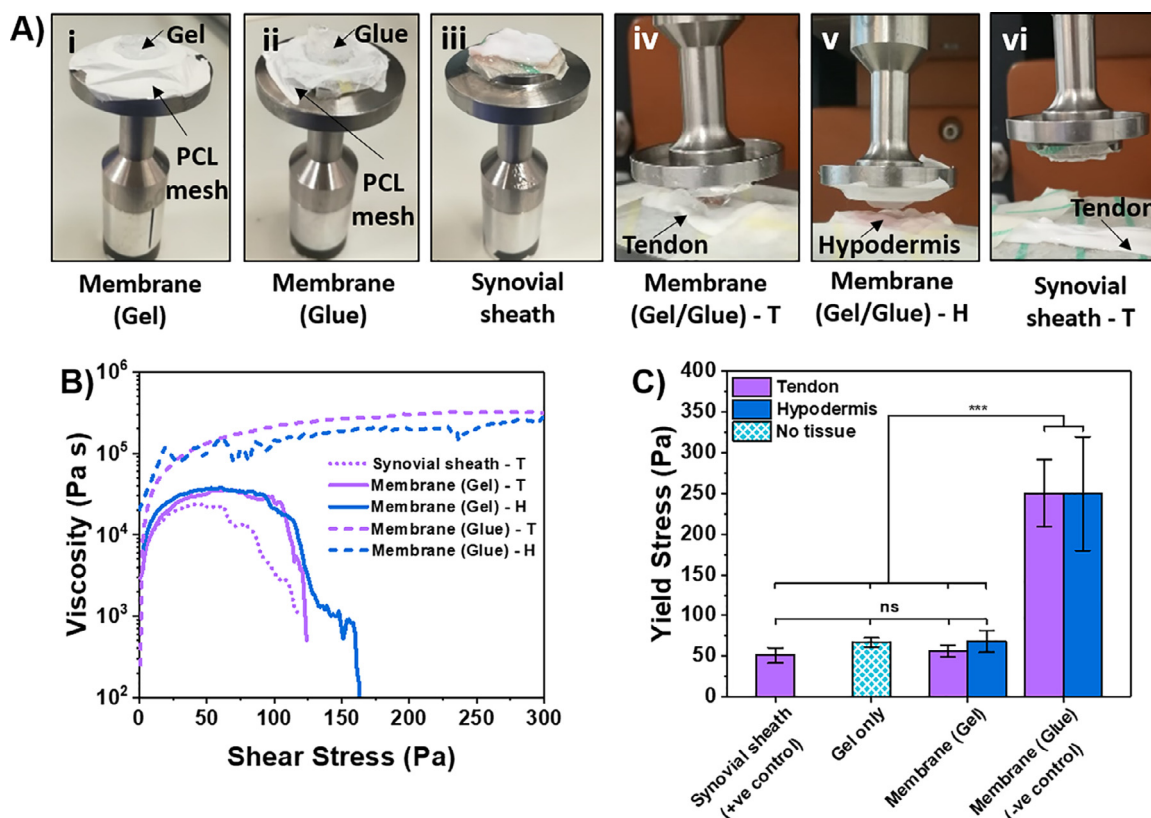


Fig. 6. Assessment of membrane lubrication properties. **A)** Experimental set-up on rheometer used to test the hydrogel ability to perform as lubricant layer. Samples to be tested were mounted on the upper head of the rheometer (i–iii), while tendon (T) and hypodermis (H) were loaded on the bottom plate (iv–vi). **B)** Representative curves of stress-ramp experiments comparing the membrane in contact with tendon (T) or hypodermis (H) tissue (synovial sheath = positive control, glue = negative control) show similar rheological behaviour for synovial sheath and the membrane. **C)** Yield stress value of the gel in contact with the plates (no tissue) was used as reference point. All measurements were performed in triplicates ($n=3$) at 37°C. (Data is shown as mean \pm SD; ***p-value < 0.001).

at 1618 cm^{-1} that, paired with a small shoulder at 1691 cm^{-1} , demonstrates anti-parallel β -sheet packing [59,60].

Rheological properties of Alpha4 hydrogel were investigated in dry conditions and after media conditioning to understand the mechanical properties that are experienced by the cells during encapsulation (dry) and cell culture (media-conditioned). Amplitude sweep experiments show that the length of the LVR is not altered by addition of culture media, even though the breaking point shifts from 28% in dry conditions to 21% in media (Fig. 5A). Moreover, addition of media results in significant decrease of storage modulus (G'), as shown in Fig. 5B (data obtained from frequency sweep experiments in Fig. ESI 4). After media conditioning (pH = 7.4), Alpha4 hydrogel has been reported to be positively charged [61]. Other studies demonstrated that neutral or positively charged SAPHS tend to increase their mechanical properties when exposed to DMEM due to charge screening and promotion of inter-chain connections, such as hydrophobic interactions and fibre bundling [32,62,63]. In this work, no such increase in mechanical properties is observed with Alpha4. This disagreement might be due to the different recipe of cell culture media utilised (Ham's F12 rather than DMEM), in particular salts and their ions, which have been reported to be the major contributors to changes in mechanical properties and self-assembly of SAPHS [62,64]. Although the mechanism behind a reduction of mechanical properties of Alpha4 upon conditioning with Ham's F12 media remains unclear, further investigations are beyond the scope of this study.

In the biomembrane, Alpha4 SAPH needs to be deposited on the PCL mesh by injection to obtain the final bilayer product. For this reason, hydrogel's recovery and shear-thinning proper-

ties were investigated via recovery and flow sweep experiments. Fig. 5C shows that, when sheared at high shear strain (100%), Alpha4 becomes liquid-like ($G' < G''$), while when the shear strain falls within the LVR (0.2%), the hydrogel recovers its solid-like behaviour ($G' > G''$), also after multiple cycles of high/low shear strain applied. Moreover, Alpha4 demonstrates shear-thinning properties (Fig. 5D), as viscosity (η) decreases with increase in shear rate ($\dot{\gamma}$). Shear-thinning behaviour is also confirmed by power law model (Eq. 2):

$$\eta = k\dot{\gamma}^{n-1} \quad (2)$$

where k is the consistency coefficient and n is the power law index; for shear-thinning materials, $0 < n < 1$ and the more shear-thinning the fluid, the closer n is to zero [65]. In Alpha4 system, the value of n is 0.02 ± 0.01 , indicating rheological properties close to those of ideally shear-thinning fluids. The shear-thinning behaviour of similar β -sheet forming SAPHS has already been reported in the literature. For example, Schneider and Pochan showed that similar peptide-based hydrogels under shear were disrupted into smaller ($\sim 200\text{ nm}$) isotropic domains, which were able to glide over each other resulting in the hydrogel to flow [66]. The formation of these domains is also responsible for the fast recovery of the hydrogel, since once the shear is removed percolation happens at the hydrogel domains' boundaries, conferring rapid recovery of initial shape and integrity [66]. Due to its recovery and shear-thinning behaviour, Alpha4 hydrogel is considered an ideal candidate for the fabrication of the anti-adhesive biomembrane.

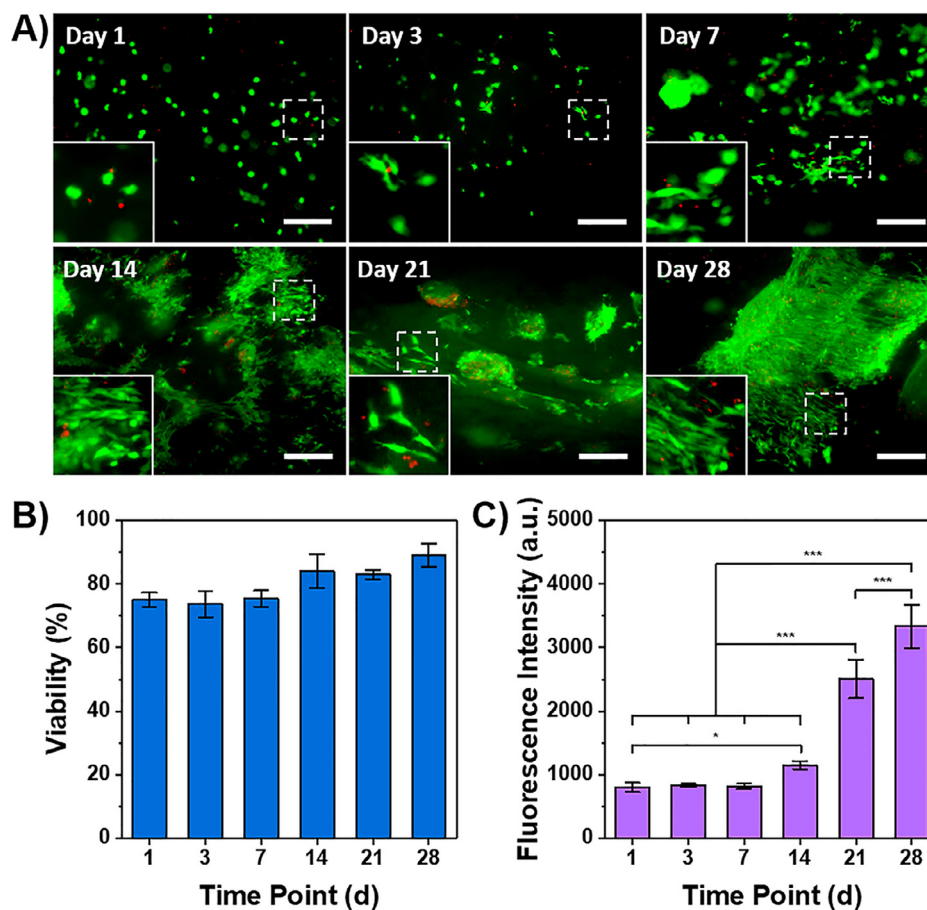


Fig. 7. HIG-82 synoviocyte behaviour upon encapsulation in Alpha4 SAPH. **A)** LIVE/DEAD assay (green = calcein AM for viable cells; red = ethidium homodimer-1 for dead cells; scale bar = 100 μm), **B)** calculation of percentage of viable cells from LIVE/DEAD images and **C)** AlamarBlue assay of HIG-82 cells upon encapsulation in Alpha4 SAPH over 28 days are shown. Alpha4 hydrogel supports sustained synoviocyte viability and proliferation during the culture period. ($n=3$; Data is shown as mean \pm SD; *p-value < 0.05; ***p-value < 0.001).

3.3. Anti-friction properties of the bilayer biomembrane

Investigating the product anti-friction properties when articulating against the tendon or the surrounding tissue is key to understand if the membrane can improve tendon gliding ability. Membrane lubrication properties on a model tissue (porcine tendon and hypodermis) were investigated by oscillatory rheology, using yield-stress measurements. This approach was adapted from a previous work performed by Stapleton *et al.*, who correlated adhesion/friction properties of hydrogels to their yield stress behaviour when articulated against a tissue [67]. In particular, the yield stress can be identified as the stress at which a fluid breaks down and starts to flow. If this concept is translated to a hydrogel that flows on a tissue, the yield stress would represent the highest friction between the biomembrane and the tendon. In this study, porcine tendon was considered an adequate model tissue due to its anatomical similarity to human tendons [68], while porcine hypodermis was used to investigate the lubrication ability of the hydrogel layer when in contact with the surrounding tissues (i.e. hypodermis).

Results in Fig. 6C show that the membrane containing the peptide hydrogel maintains the same yield stress whether it is on tissue or not, indicating that gliding happens due to mechanical failure occurring within the hydrogel layer (cohesive yielding) rather than adhesion failure at the interface between the tissue (tendon or hypodermis) and the hydrogel. According to Stapleton *et al.*, cohesive yielding paired with recovery and shear-thinning properties

(as shown in Fig. 5C-D) suggest that the hydrogel layer could be smeared or spread on the tissue surface without delaminating [67]. This results in the hydrogel being able to flow when a shear stress is applied during tendon movement without detaching from the target tissue [67]. In addition, since the hydrogel rapidly recovers its solid-like behaviour after flowing, it can be argued that the hydrogel quickly adheres and settles on the tissue surface [67].

The lubrication properties of the membrane are also confirmed by the yield stress behaviour of the membrane compared to the synovial sheath (Fig. 6). Indeed, the shear stress at which the synovial sheath starts to glide on the tendon (50.95 ± 9.24 Pa) is not statistically different from that of the biomembrane (PCL+hydrogel) on the tendon (55.97 ± 7.15 Pa). Moreover, the fingerprint of the viscosity-shear stress curves is similar (Fig. 6B), indicating that the friction forces at tendon-membrane interface are physiologically comparable. The presence of a yield point in the viscosity curve is fundamental to start the breakdown of the hydrogel layer and consequent gliding. A silicone glue used as a negative control (Fig. 6A ii) shows no yielding behaviour and increased viscosity, resulting in no motion at the interface between glue and tissue.

Mobilisation after tendon repair is considered one of the most important means to minimise adhesion formation and restore normal gliding ability after surgery [8,9]. In order to improve post-surgery outcomes, it is imperative to adopt rehabilitation regimes promptly after operation with early-active programmes [5,69]. The presence of a membrane between the tendon and surrounding tis-

sue should support early-active mobilisation. For this reason, the anti-friction properties of the acellular product are key to evaluate tendon gliding and facilitate short-term functionality.

3.4. Encapsulation of synoviocytes in Alpha4 for long-term regeneration

The membrane described in this work has the capability to prevent infiltration of fibroblasts and provide short-term lubrication. However, in its acellular form, it does not assist in the regeneration of the tendon synovial sheath. Therefore, introducing a cellular component in the hydrogel layer could be potentially exploited to achieve effective repair of the synovial sheath by recapitulating the native matrix through deposition of essential ECM components. In particular, type-B synoviocytes are involved in endocrine and sensory function of synovial sheath, as well as production of specialised matrix components including HA and collagen fibres within the intimal interstitium and synovial fluid [11]. For this reason, the incorporation of type-B synoviocytes in a tis-

sue engineered construct would be particularly appealing to obtain improved regeneration and functionality in the long term. Within the tendon synovial sheath, type-B synoviocytes play a key role for lubrication at the interface of two tissues, being responsible for the production of HA [70]. For this reason, HIG-82s, a continuous cell line obtained from knee synovium of rabbits [71] that resembles type-B synoviocytes, was used in this study to provide proof-of-concept of improved biomembrane functionality in the long term through cell encapsulation in Alpha4-covered PCL mesh.

Cells were encapsulated in Alpha4 hydrogel and cultured for 28 days. Synoviocyte viability remains high throughout the entire period of culture (Fig. 7B), showing an increased density of live cells forming clusters from day 14 onwards (Fig. 7A). Within the first 72 hours of 3D culture, HIG-82s exhibit a rounded shape (Fig. 7A) and metabolic activity remains stable (Fig. 7C), probably due to the rearrangement of cells and adaptation to the new 3D environment. Characteristic spindle-like morphology of synoviocytes starts to be visible after 7 days of encapsulation, while after 2 weeks the elongated morphology is also accompanied by

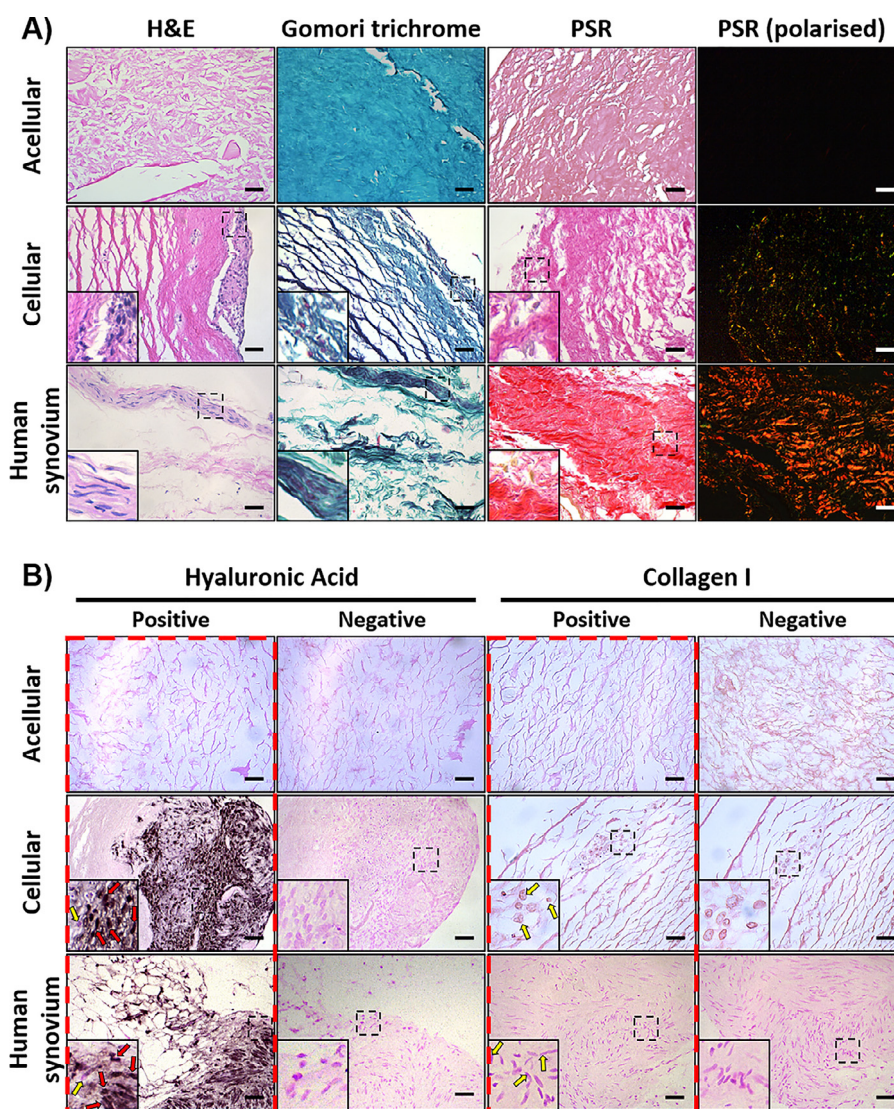


Fig. 8. Histological assessment of HIG-82 synoviocytes encapsulated in Alpha4 hydrogel after 28 days (Cellular) compared to acellular controls and human synovium tissue. A) H&E shows that synoviocytes deposit their own ECM and form a compact and dense layer resembling the cellular organisation of the intimal layer in the human synovium. Gomori trichrome and PSR for collagen detection indicate deposition of collagen fibres (PSR staining under polarised light shows birefringence; green = type-III collagen, red = type-I collagen). B) Immunohistochemical detection of HA and type-I collagen indicates that synoviocytes produce HA in the pericellular matrix but not type-I collagen, mimicking human synovium composition. Positive (enclosed in red dashed boxes) = construct/tissue exposed to primary antibody; Negative = construct/tissue not exposed to primary antibody. Red arrows point at immunopositive cells, while yellow arrows point at immunonegative cells. (Scale bar = 50 μ m).

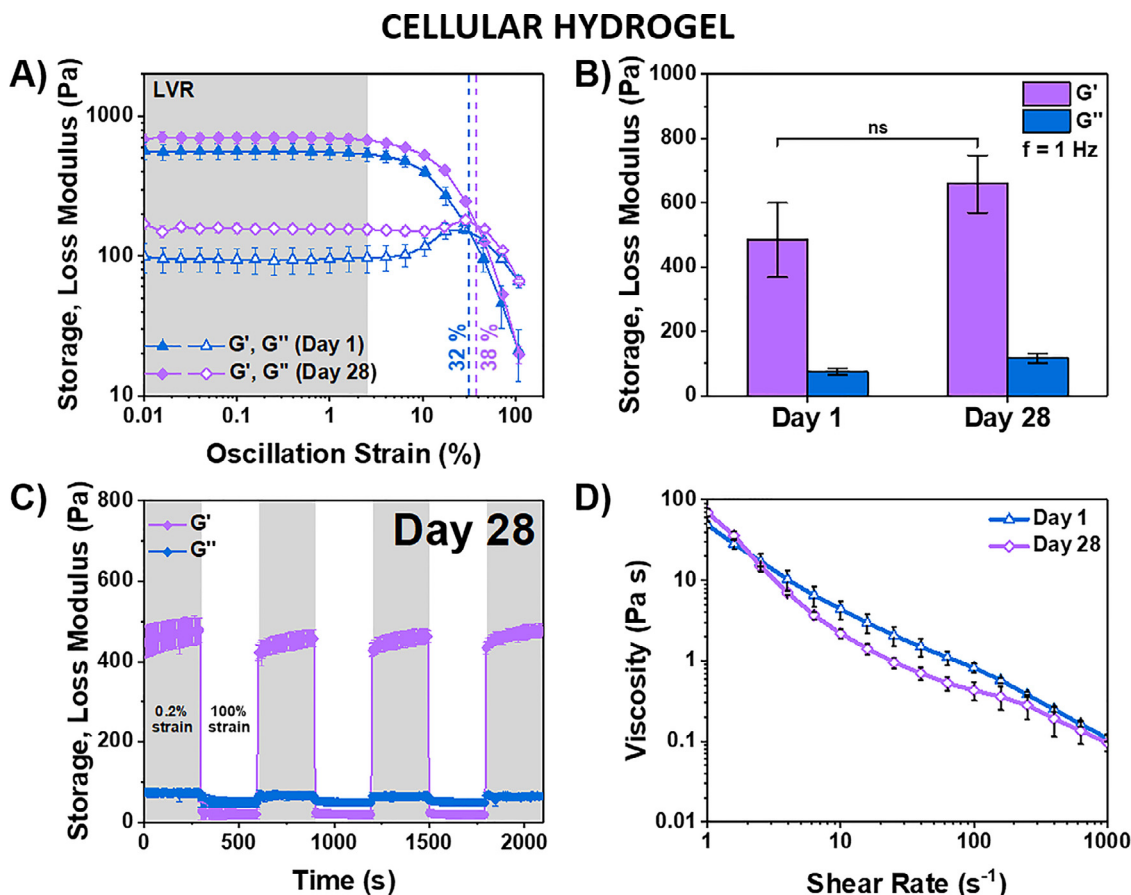


Fig. 9. Oscillatory shear rheology of HIG-82 synoviocyte-laden Alpha4 SAPH constructs over 28 days of culture. **A)** Mechanical properties of the hydrogel were tested via amplitude sweep experiments performed after 1 day and 28 days of culture. The grey area indicates the LVR region. **B)** Average values of storage and loss moduli of hydrogel at 1 Hz after 1 day and 28 days of culture describe the network visco-elasticity properties of the cell-hydrogel constructs. **C)** Recovery experiments with low (0.2%, grey areas) and high (100%, white areas) strain deformation at day 28 of culture and **D)** flow sweep experiments after 1 day and 28 days of culture show self-healing and shear-thinning properties of the hydrogel. All measurements were performed in triplicates ($n=3$) at 37°C. (Data is shown as mean \pm SD; ^{ns}p-value > 0.05).

a significant increase in metabolic activity (1.4-fold) compared to day 7. After 3 and 4 weeks of culture, the metabolic activity continues to grow, showing a significant increase compared to week 1 of culture (3-fold and 4-fold increase after 21 and 28 days respectively). These results suggest that Alpha4 provides an ECM-like environment, which is able to promote synoviocyte growth and proliferation by providing a suitable platform for 3D cell culture of this cell line. Other ionic-complementary SAPHs have been used for different tissue engineering (TE) applications [30,72,73], but the use of these hydrogels as niches and cell carriers for tendon TE is still in its infancy. Recently, Yin *et al.* have demonstrated that RADA peptide hydrogels and their RGD-functionalised counterparts recapitulate the specific features of tendon 3D microenvironment, with the effect of rejuvenating aged/degenerative human tendon stem/progenitor cells [74]. These hydrogels created a nano- and micro-fibrous network that resembled that of the native tendon tissue, guiding aged/degenerative cells to recover the phenotype typical of younger cells [74].

In order to evaluate whether Alpha4 hydrogel can be considered as a good candidate to offer a suitable ECM microenvironment for encapsulated synoviocytes, cell-laden constructs were tested for deposition of specific matrix components, in particular collagens and HA. Indeed, it is imperative that the hydrogel layer supports endogenous production of HA to ensure prolonged restoration of tendon gliding after degradation of the hydrogel phase *in vivo*. In fact, as shown in Fig. ESI 5, Alpha4 hydrogel degrades *in vitro* probably due to bulk erosion of the hydrogel network [75]. Addi-

tionally, the incorporation of synoviocytes caused an average increase in the degradation level (+14% in weight loss over 28 days) compared to acellular hydrogels, indicating an involvement of encapsulated cells in the degradation of the hydrogel constructs due to enzymatic activity [34]. These results suggest that the hydrogel implanted *in vivo* may experience degradation due to a combination of physical erosion and cellular activity.

Overall, synoviocytes encapsulated in Alpha4 hydrogel show visible ECM deposition after 4 weeks of culture (Fig. 8A). H&E staining shows that cells formed a compact and dense layer resembling the cellular organisation of human synovium in the intimal layer [76]. Although the hydrogel tends to be stained, collagen fibres can be observed with Gomori trichrome and PSR staining and distinguished from the peptide matrix. In particular, looking at PSR staining under polarised light, it is possible to observe that type-III collagen is deposited by synoviocytes, recapitulating the content of collagen in the intimal matrix of human synovium [76]. Similarly to the content of human synovium, very little amount of type-I collagen is produced, as confirmed by immunohistochemistry detection of the protein (Fig. 8B). These outcomes would suggest that the cells encapsulated in Alpha4 SAPH would not contribute to the process of adhesion formation, since scarring and fibrosis rely on type-I collagen deposition for tissue repair [15].

HA production by synoviocytes was also evaluated with immunostaining (Fig. 8B) and Alcian Blue staining according to Scott method (Fig. ESI 6). Alpha4 is conducive to deposition of HA, which is predominant in the pericellular matrix. Immunopositive

cells are observed after 28 days of culture (Fig. 8B), indicating that at that time point synoviocytes have not only produced and deposited HA around them, but they are still in the process of HA production at cellular level. These outcomes indicate that synoviocytes encapsulated in Alpha4 hydrogel produce a matrix that is reminiscent of that of the native tissue, since the staining pattern closely resembles that of the human synovium. Consequently, it can be argued that the proposed biomembrane has the potential to ensure long-term lubrication due to the constant and prolonged production of HA, which in turn could help to restore and maintain tendon functionality. The incorporation of an endogenous source of HA could potentially substitute the hydrogel in its role as lubricant after degradation, ensuring low friction properties also in the late stages of tendon healing [35]. The proposed biomembrane represents an alternative and unique approach for the treatment of tendon adhesions because it offers a way to overcome the issues typical of commercial anti-adhesion membranes.

In terms of mechanical behaviour, the incorporation of synoviocytes and their deposition of ECM do not significantly alter the overall rheological properties of the hydrogel. Indeed, G' and G'' in acellular hydrogels conditioned with media (Fig. 5A–B) and cellular gels at day 28 (Fig. 9A–B) are comparable. On the contrary, a difference in G' was observed between media-conditioned acellular hydrogels and cell-laden constructs at day 1, probably due to a rearrangement of the peptide chains as result of the perturbation caused by the incorporation of cells. This potentially leads to a more heterogeneous 3D network having lower capacity to store energy compared to acellular counterparts. Although hydrogel degradation is observed in cell-laden hydrogels over the 28-days observation period, a slight increase in G' can be detected after 28 days of culture compared to day 1 (Fig. 9A and B, whose data were obtained from frequency sweep experiments shown in Fig. ESI 7), although this difference is not statistically significant. This increase in G' is probably due to an effect of the *de novo* tissue, which compensates the difference in mechanical properties observed between acellular and cellular hydrogels after day 1 of culture. Indeed, cells are able to remodel the surrounding network, degrading and replacing it with newly deposited ECM deposition, as shown in Fig. 8. Comparing recovery cycles in acellular gels and cellular constructs at both day 1 and 28, it is possible to notice a significant difference in G' values. This difference is due to testing conditions, since acellular hydrogels reported in Fig. 5C were tested in 'dry' status, while cellular constructs (Fig. 9C and Fig. ESI 8) were buffered with media. Interestingly, the self-healing and shear-thinning behaviour of Alpha4 hydrogel is retained also after cell encapsulation and media conditioning, as demonstrated in Fig. 9C–D and Fig. ESI 8. These outcomes suggest that the performance of the cell-laden constructs would be comparable to that of the acellular hydrogels described in Fig. 6 if articulated against the tendon tissue. Therefore, it could be speculated that the presence of synoviocytes does not alter the ability of the hydrogel layer to act as lubricant, without delaminating or leaving the tissue target.

For clinical translation, we envisage that this bilayer membrane could be sutured in place in the first instance and, once in situ, fibrous adhesion between the hypodermis and the PCL mesh would also hold it in place. Specifically, the bilayer scaffold would be carefully sutured between the pulleys, to reform the flexor tendon sheath, so that the gliding layer is interacting with tendon and the adherent PCL surface is in contact with the hypodermis. In sites where pulleys are absent, the bilayer biomembrane would be sutured onto the hypodermis, so that, when the skin is closed, the scaffold would form a wrap around the tendon. The skin closure would ensure that the membrane is adherent to the hypodermis (on the PCL side), whereas the gliding layer (hydrogel) would produce an artificial flexor tendon sheath replacement. Over a few minutes, the PCL mesh would be adherent to the hypodermis due

to fibrin forming on its raw surface. This would provide enough strength to resist the force needed to induce gliding within the hydrogel layer.

4. Conclusion

This study constitutes a proof-of-concept that could potentially overcome the current issues of fast degradation, short-term effectiveness and poor synovial sheath regeneration related to acellular non-biomimetic anti-adhesion barriers. To achieve this, we proposed a bilayer biomembrane to be wrapped around the tendon, composed of a nanofibrous PCL mesh and Alpha4 SAPH. The PCL mesh acted as a physical barrier to adhesion-forming fibroblasts, suggesting prevention of peritendinous adhesions after surgery. Addition of the hydrogel layer to the polymeric membrane provided anti-friction properties to the tendon comparable to those found in physiological conditions (native synovial sheath), indicating that smooth movement of the tendon could be achieved upon membrane implantation. Moreover, a biologically active component was introduced into the biomembrane by incorporating type-B synoviocytes. In a clinical scenario, this cellular component would be an added value to facilitate tendon motion through the fibro-osseous cavity, after *in vivo* dissolution of the SAPH. In fact, the presence of type-B synoviocytes allowed the production of a *de novo* matrix, which could compensate any degradation of the hydrogel phase and actively contribute to the process of synovial sheath repair. The prolonged secretion of endogenous HA by synoviocytes could potentially improve tendon functionality in the long term. Further experiments are currently being carried out to assess the lubrication and gliding ability of the cell-laden hydrogel/PCL membrane *in vitro* and *ex vivo*. Furthermore, future *in vivo* studies are under consideration to further assess the performance of the system under relevant physiological conditions. Finally, we envisage that the bilayer biomembrane model proposed in this work could also find application as post-operative tool to tackle adhesion formation also in other tissue targets, such as intra-abdominal and gynaecological areas.

Declaration of Competing Interest

The authors declare that they have no known competing financial interests or personal relationships that could have appeared to influence the work reported in this paper.

Acknowledgements

The authors acknowledge the Engineering and Physical Sciences Research Council (EPSRC) and Medical Research Council Centre for Doctoral Training in Regenerative Medicine for funding this study (EP/L014904/1). This work was also supported by the Henry Royce Institute for Advanced Materials, funded through EPSRC grants EP/R00661X/1, EP/S019367/1, EP/P025021/1 and EP/P025498/1. The authors thank the University of Liverpool and Liverpool Musculoskeletal Biobank for sourcing the human synovium tissue used in this study.

Supplementary materials

Supplementary material associated with this article can be found, in the online version, at doi:10.1016/j.actbio.2020.11.017.

References

- [1] N. Fitzpatrick, L. Finlay, Frustrating disability": The lived experience of coping with the rehabilitation phase following flexor tendon surgery, *Int. J. Qual. Stud. Health Well-Being*. 3 (2008) 143–154, doi:10.1080/17482620802130407.

- [2] S. Rawson, S. Cartmell, J. Wong, Suture techniques for tendon repair; a comparative review, *Muscles. Ligaments Tendons J.* 3 (2013) 220–228, doi:10.11138/mltj/2013.3.3.220.
- [3] R.H. Caulfield, A. Maleki-Tabrizi, H. Patel, F. Coldham, S. Mee, J. Nanchahal, Comparison of zones 1 to 4 flexor tendon repairs using absorbable and unabsorbable four-strand core sutures., *J. Hand Surg. Eur.* 33 (2008) 412–417, doi:10.1177/1753193408090758.
- [4] A. Momeni, E. Grauel, J. Chang, Complications After Flexor Tendon Injuries, *Hand Clin* 26 (2010) 179–189, doi:10.1016/j.hcl.2009.11.004.
- [5] A. Khanna, N. Gougoulis, N. Maffulli, Modalities in prevention of flexor tendon adhesion in the hand : What have we achieved so far? *Acta Orthopædica Belgica* 75 (2009) 433–444.
- [6] M.B. Geary, C.A. Orner, F. Bawany, H.A. Awad, W.C. Hammert, R.J. O'Keefe, A.E. Loiselle, Systemic EP4 Inhibition Increases Adhesion Formation in a Murine Model of Flexor Tendon Repair, *PLoS One* 10 (2015) e0136351 – e0136351, doi:10.1371/journal.pone.0136351.
- [7] M.A.T. Freeberg, A. Easa, J.A. Lillis, D.S.W. Benoit, A.J. van Wijnen, H.A. Awad, Transcriptomic Analysis of Cellular Pathways in Healing Flexor Tendons of Plasminogen Activator Inhibitor 1 (PAI-1/Serpine1) Null Mice, *J. Orthop. Res.* 38 (2020) 43–58, doi:10.1002/jor.24448.
- [8] P.C. Amadio, Friction of the gliding surface: Implications for tendon surgery and rehabilitation, *J. Hand Ther* 18 (2005) 112–119, doi:10.1197/j.jht.2005.01.005.
- [9] A. Khanna, M. Friel, N. Gougoulis, U.G. Longo, N. Maffulli, Prevention of adhesions in surgery of the flexor tendons of the hand : what is the evidence ? *Br. Med. Bull.* 90 (2009) 85–109, doi:10.1093/bmb/ldp013.
- [10] M. Benjamin, E. Kaiser, S. Milz, Structure-function relationships in tendons: A review, *J. Anat.* 212 (2008) 211–228, doi:10.1111/j.1469-7580.2008.00864.x.
- [11] T. Iwanaga, M. Shikichi, H. Kitamura, H. Yanase, K. Nozawa-Inoue, Morphology and functional roles of synoviocytes in the joint, *Arch. Histol. Cytol.* 63 (2000) 17–31, doi:10.1679/aohc.63.17.
- [12] R. St Onge, C. Weiss, J.L. Denlinger, E.A. Balazs, A preliminary assessment of Na-hyaluronate injection into "no man's land" for primary flexor tendon repair, *Clin. Orthop. Relat. Res.* (1980) 269–275.
- [13] G. Hanff, S.O. Abrahamsson, Matrix synthesis and cell proliferation in repaired flexor tendons within e-PtFE reconstructed flexor tendon sheaths, *J. Hand Surg. Eur.* 21 (1996) 642–646, doi:10.1016/S0266-7681(96)80149-5.
- [14] D. Docheva, S.A. Müller, M. Majewski, C.H. Evans, Biologics for tendon repair, *Adv. Drug Deliv. Rev.* 84 (2015) 222–239, doi:10.1016/j.addr.2014.11.015.
- [15] J.K.F. Wong, Y.H. Lui, Z. Kapacee, K.E. Kadler, M.W.J. Ferguson, D.A. McGrouther, The Cellular Biology of Flexor Tendon Adhesion Formation. An Old Problem in a New Paradigm, *Am. J. Pathol.* 175 (2009) 1938–1951, doi:10.2353/ajpath.2009.090380.
- [16] H. Capella-Monsonis, S. Kearns, J. Kelly, D.I. Zeugolis, Battling adhesions: from understanding to prevention, *BMC Biomed. Eng.* 1 (2019) 5, doi:10.1186/s42490-019-0005-0.
- [17] G. Trew, Postoperative adhesions and their prevention, *Rev. Gynaecol. Perinat. Pract.* 6 (2006) 47–56, doi:10.1016/j.rigapp.2006.02.001.
- [18] R.L. DeWilde, G. Trew, Postoperative abdominal adhesions and their prevention in gynaecological surgery. Expert consensus position. Part 2 - Steps to reduce adhesions, *Gynecol. Surg.* 4 (2007) 243–253, doi:10.1007/s10397-007-0333-2.
- [19] V.W. Fazio, Z. Cohen, J.W. Fleshman, H. Van Goor, J.J. Bauer, B.G. Wolff, M. Cormann, R.W. Beart, S.D. Wexner, J.M. Becker, J.R.T. Monson, H.S. Kaufman, D.E. Beck, H.R. Bailey, K.A. Ludwig, M.J. Stamos, A. Darzi, R. Bleday, R. Dorazio, R.D. Madoff, L.E. Smith, S. Gearhart, K. Lillemo, J. Göhl, Reduction in adhesive small-bowel obstruction by Sefrafilm® adhesion barrier after intestinal resection, *Dis. Colon Rectum.* 49 (2006) 1–11, doi:10.1007/s10350-005-0268-5.
- [20] M. Naito, N. Ogura, T. Yamanashi, T. Sato, T. Nakamura, H. Miura, A. Tsutsui, Y. Sakamoto, R. Tanaka, Y. Kumagai, M. Watanabe, Prospective randomized controlled study on the validity and safety of an absorbable adhesion barrier (Interceed(R)) made of oxidized regenerated cellulose for laparoscopic colorectal surgery. PG - 7-11 LID - 10.1111/ases.12334 [doi], (n.d.).
- [21] G.H. Trew, G.A. Pistofidis, S.Y. Brucker, B. Krämer, N.M. Ziegler, M. Korrell, H. Ritter, A. McConnachie, I. Ford, A.M. Crowe, T.D. Estridge, M.P. Diamond, R.L. De Wilde, A first-in-human, randomized, controlled, subject- and reviewer-blinded multicenter study of Actamax™ Adhesion Barrier, *Arch. Gynecol. Obstet* 295 (2017) 383–395, doi:10.1007/s00404-016-4211-x.
- [22] C. Farquhar, P. Vandekerckhove, A. Watson, A. Vail, D. Wiseman, Barrier agents for preventing adhesions after surgery for subfertility, in: C. Farquhar (Ed.), *Cochrane Database Syst. Rev.*, John Wiley & Sons, Ltd, Chichester, UK, 1999, doi:10.1002/14651858.CD000475.
- [23] A.F. Haney, J. Hesla, B.S. Hurst, L.M. Kettel, A.A. Murphy, J.A. Rock, G. Rowe, W.D. Schlaff, Expanded polytetrafluoroethylene (Gore-Tex Surgical Membrane) is superior to oxidized regenerated cellulose (Interceed TC7) in preventing adhesions, *Fertil. Steril.* 63 (1995) 1021–1026, doi:10.1016/S0015-0282(16)57541-4.
- [24] S.H. Chen, C.H. Chen, Y.T. Fong, J.P. Chen, Prevention of peritendinous adhesions with electrospun chitosan-grafted polycaprolactone nanofibrous membranes, *Acta Biomater* 10 (2014) 4971–4982, doi:10.1016/j.actbio.2014.08.030.
- [25] S.H. Chen, C.H. Chen, K.T. Shalumon, J.P. Chen, Preparation and characterization of antiadhesion barrier film from hyaluronic acid-grafted electrospun poly(caprolactone) nanofibrous membranes for prevention of flexor tendon postoperative peritendinous adhesion, *Int. J. Nanomedicine.* 9 (2014) 4079–4092, doi:10.2147/IJN.S67931.
- [26] K. Amin, R. Moscalu, A. Imere, R. Murphy, S. Barr, Y. Tan, R. Wong, P. Sorooshian, F. Zhang, J. Stone, J. Fildes, A. Reid, J. Wong, The future application of nanomedicine and biomimicry in plastic and reconstructive surgery, *Nanomedicine* 14 (2019) 2679–2696, doi:10.2217/nmm-2019-0119.
- [27] C.H. Chen, S.H. Chen, K.T. Shalumon, J.P. Chen, Prevention of peritendinous adhesions with electrospun polyethylene glycol/polycaprolactone nanofibrous membranes, *Colloids Surfaces B Biointerfaces* 133 (2015) 221–230, doi:10.1016/j.colsurfb.2015.06.012.
- [28] S. Jiang, H. Yan, D. Fan, J. Song, C. Fan, Multi-layer electrospun membrane mimicking tendon sheath for prevention of tendon adhesions, *Int. J. Mol. Sci.* 16 (2015) 6932–6944, doi:10.3390/ijms16046932.
- [29] P.Y. Chou, S.H. Chen, C.H. Chen, S.H. Chen, Y.T. Fong, J.P. Chen, Thermo-responsive in-situ forming hydrogels as barriers to prevent post-operative peritendinous adhesion, *Acta Biomater* 63 (2017) 85–95, doi:10.1016/j.actbio.2017.09.010.
- [30] L.A. Castillo Diaz, A. Saiani, J.E. Gough, A.F. Miller, Human osteoblasts within soft peptide hydrogels promote mineralisation in vitro, *J. Tissue Eng* 5 (2014) 204173141453934, doi:10.1177/2041731414539344.
- [31] J. Zhu, R.E. Marchant, Design properties of hydrogel tissue-engineering scaffolds, *Expert Rev. Med. Devices.* 8 (2011) 607–626, doi:10.1586/erd.11.27.
- [32] C. Ligorio, M. Zhou, J.K. Wychowanec, X. Zhu, C. Bartlam, A.F. Miller, A. Vijayaraghavan, J.A. Hoyland, A. Saiani, Graphene oxide containing self-assembling peptide hybrid hydrogels as a potential 3D injectable cell delivery platform for intervertebral disc repair applications, *Acta Biomater* 92 (2019) 92–103, doi:10.1016/j.actbio.2019.05.004.
- [33] F. Gelain, D. Bottai, A. Vescovi, S. Zhang, Designer Self-Assembling Peptide Nanofiber Scaffolds for Adult Mouse Neural Stem Cell 3-Dimensional Cultures, *PLoS One* 1 (2006) e119, doi:10.1371/journal.pone.0000119.
- [34] O. Morris, M.A. Elsayy, M. Fairclough, K.J. Williams, A. McMahon, J. Grigg, D. Forster, A.F. Miller, A. Saiani, C. Prent, In vivo characterisation of a therapeutically relevant self-assembling 18F-labelled β -sheet forming peptide and its hydrogel using positron emission tomography, *J. Label. Compd. Radiopharm.* 60 (2017) 481–488, doi:10.1002/jlcr.3534.
- [35] A.M. Ozturk, A. Yam, I.C. Song, S.H. Tan, F. Helvacoglu, A. Tan, Synovial cell culture and tissue engineering of a tendon synovial cell biomembrane, *J. Biomed. Mater. Res. - Part A.* 84 (2008) 1120–1126, doi:10.1002/jbm.a.31738.
- [36] M.S. Kim, J. Son, H. Lee, H. Hwang, C.H. Choi, G. Kim, Highly porous 3D nanofibrous scaffolds processed with an electrospinning/laser process, *Curr. Appl. Phys.* 14 (2014) 1–7, doi:10.1016/j.cap.2013.10.008.
- [37] F. Croisier, A.-S. Duvez, C. Jerome, A.F. Leonard, K.O. van der Werf, P.J. Dijkstra, M.L. Bennink, Mechanical testing of electrospun PCL fibers, *Acta Biomater* 8 (2012) 218–224, doi:10.1016/j.actbio.2011.08.015.
- [38] L. Bosworth, N. Alam, J. Wong, S. Downes, Investigation of 2D and 3D electrospun scaffolds intended for tendon repair, *J. Mater. Sci. Mater. Med.* 24 (2013) 1605–1614, doi:10.1007/s10856-013-4911-8.
- [39] L.-K. Huang, M.-J.J. Wang, Image thresholding by minimizing the measures of fuzziness, *Pattern Recognit* 28 (1995) 41–51, doi:10.1016/0031-3203(94)E0043-K.
- [40] S. Uchiyama, J.H. Coert, L. Berglund, P.C. Amadio, K.-N. An, Method for the measurement of friction between tendon and pulley, *J. Orthop. Res.* 13 (1995) 83–89, doi:10.1002/jor.1100130113.
- [41] R. Wu, B.M. Sansbury, D. Man, Fabrication and Evaluation of Multilayer Nanofiber-Hydrogel Meshes with a Controlled Release Property, *Fibers* 3 (2015) 296–308, doi:10.3390/fib3030296.
- [42] S. Sánchez-González, N. Diban, A. Urtiaga, Hydrolytic Degradation and Mechanical Stability of Poly(ϵ -Caprolactone)/Reduced Graphene Oxide Membranes as Scaffolds for In Vitro Neural Tissue Regeneration, *Membranes (Basel)* 8 (2018) 12, doi:10.3390/membranes8010012.
- [43] N. Bölgel, Y.Z. Menceloğlu, K. Acatur, I. Vargel, E. Pişkin, In vitro and in vivo degradation of non-woven materials made of poly(epsilon-caprolactone) nanofibers prepared by electrospinning under different conditions., *J. Biomater. Sci. Polym. Ed.* 16 (2005) 1537–1555, doi:10.1163/156856205774576655.
- [44] A.L. Titan, D.S. Foster, J. Chang, M.T. Longaker, Flexor Tendon, Development, Healing, Adhesion Formation, and Contributing Growth Factors, *Plast. Reconstr. Surg.* 144 (2019) 639e–647e, doi:10.1097/PRS.0000000000006048.
- [45] E. Yurdakul Sikar, H.E. Sikar, H. Top, A.C. Aygıt, Effects of Hyalobarrier gel and Sefrafilm in preventing peritendinous adhesions following crush-type injury in a rat model, *Ulus. Travma Acil Cerrahi Derg.* 25 (2019) 93–98, doi:10.5505/tjtes.2018.54007.
- [46] J. Rnjak-Kovacina, A.S. Weiss, Increasing the Pore Size of Electrospun Scaffolds, *Tissue Eng. Part B Rev.* 17 (2011) 365–372, doi:10.1089/ten.teb.2011.0235.
- [47] Q.P. Pham, U. Sharma, A.G. Mikos, Electrospun Poly(ϵ -caprolactone) Microfiber and Multilayer Nanofiber/Microfiber Scaffolds: Characterization of Scaffolds and Measurement of Cellular Infiltration, *Biomacromolecules* 7 (2006) 2796–2805, doi:10.1021/bm060680j.
- [48] S.J. Eichhorn, W.W. Sampson, Statistical geometry of pores and statistics of porous nanofibrous assemblies, *J. R. Soc. Interface.* 2 (2005) 309–318, doi:10.1098/rsif.2005.0039.
- [49] A. Balguid, A. Mol, M.H. van Marion, R.A. Bank, C.V.C. Bouten, F.P.T. Baaijens, Tailoring Fiber Diameter in Electrospun Poly(ϵ -Caprolactone) Scaffolds for Optimal Cellular Infiltration in Cardiovascular Tissue Engineering, *Tissue Eng. Part A.* 15 (2008) 437–444, doi:10.1089/ten.tea.2007.0294.
- [50] S. Soliman, S. Sant, J.W. Nichol, M. Khabiry, E. Traversa, A. Khademhosseini, Controlling the porosity of fibrous scaffolds by modulating the fiber diameter and packing density, *J. Biomed. Mater. Res. Part A.* 96A (2011) 566–574, doi:10.1002/jbm.a.33010.

- [51] J. Wu, Y. Hong, Enhancing cell infiltration of electrospun fibrous scaffolds in tissue regeneration, *Bioact. Mater.* 1 (2016) 56–64, doi:10.1016/j.bioactmat.2016.07.001.
- [52] D. Kumar, V. Workman, M. Obrien, J. McLaren, L. White, K. Ragunath, F.R.A.J. Rose, A. Saiani, J. Gough, Peptide Hydrogels-A Tissue Engineering Strategy for the Prevention of Oesophageal Strictures, *Adv. Funct. Mater.* 27 (2017) 1702424, doi:10.1002/adfm.201702424.
- [53] C. Yan, M.E. Mackay, K. Czymmek, R.P. Nagarkar, J.P. Schneider, D.J. Pochan, Injectable solid peptide hydrogel as a cell carrier: effects of shear flow on hydrogels and cell payload, *Langmuir* 28 (2012) 6076–6087, doi:10.1021/la2041746.
- [54] A. Mata, Y. Geng, K.J. Henrikson, C. Aparicio, S.R. Stock, R.L. Satcher, S.I. Stupp, Bone regeneration mediated by biomimetic mineralization of a nanofiber matrix, *Biomaterials* 31 (2010) 6004–6012, doi:10.1016/j.biomaterials.2010.04.013.
- [55] V.A. Kumar, N.L. Taylor, S. Shi, N.C. Wickremasinghe, R.N. D'Souza, J.D. Hartgerink, Self-assembling multidomain peptides tailor biological responses through biphasic release, *Biomaterials* 52 (2015) 71–78, doi:10.1016/j.biomaterials.2015.01.079.
- [56] S. Koutsopoulos, L.D. Unsworth, Y. Nagai, S. Zhang, Controlled release of functional proteins through designer self-assembling peptide nanofiber hydrogel scaffold, *Proc. Natl. Acad. Sci.* 106 (2009) 4623 LP-4628, doi:10.1073/pnas.0807506106.
- [57] C. Tang, A.F. Miller, A. Saiani, Peptide hydrogels as mucoadhesives for local drug delivery, *Int. J. Pharm.* 465 (2014) 427–435, doi:10.1016/j.ijpharm.2014.02.039.
- [58] D.M. Marini, W. Hwang, D.A. Lauffenburger, S. Zhang, R.D. Kamm, Left-Handed Helical Ribbon Intermediates in the Self-Assembly of a β -Sheet Peptide, *Nano Lett* 2 (2002) 295–299, doi:10.1021/nl015697g.
- [59] A.F. Miller, A. Saiani, Engineering peptide based biomaterials: Structure, properties and application, *Chim. Oggi* 28 (2010) 34–38.
- [60] A. Barth, Infrared spectroscopy of proteins, *Biochim. Biophys. Acta - Bioenerg.* 1767 (2007) 1073–1101. 10.1016/j.bbabi.2007.06.004.
- [61] Manchester BIOGEL, PeptiGels® - Hydrogel products, (n.d.). <https://manchesterbiogel.com/products/peptigels> (accessed April 22, 2020).
- [62] F. Koch, M. Müller, F. König, N. Meyer, J. Gattlen, U. Pielas, K. Peters, B. Kreikemeyer, S. Mathes, S. Saxer, Mechanical characteristics of beta sheet-forming peptide hydrogels are dependent on peptide sequence, concentration and buffer composition, *R. Soc. Open Sci.* 5 (2018) 171562, doi:10.1098/rsos.171562.
- [63] M.R. Caplan, P.N. Moore, S. Zhang, R.D. Kamm, D.A. Lauffenburger, Self-assembly of a beta-sheet protein governed by relief of electrostatic repulsion relative to van der Waals attraction, *Biomacromolecules* 1 (2000) 627–631, doi:10.1021/bm005586w.
- [64] B. Ozbas, J. Kretsinger, K. Rajagopal, J.P. Schneider, D.J. Pochan, Salt-triggered peptide folding and consequent self-assembly into hydrogels with tunable modulus, *Macromolecules* 37 (2004) 7331–7337, doi:10.1021/ma0491762.
- [65] J.W. Goodwin, R.W. Hughes, Chapter 1 Introduction, in: *Rheol. Chem. An Introd.*, 2nd ed., The Royal Society of Chemistry, 2008, p. 6, doi:10.1039/9781847558046-00001.
- [66] C. Yan, A. Altunbas, T. Yucel, R.P. Nagarkar, J.P. Schneider, D.J. Pochan, Injectable solid hydrogel: mechanism of shear-thinning and immediate recovery of injectable β -hairpin peptide hydrogels, *Soft Matter* 6 (2010) 5143–5156, doi:10.1039/C0SM00642D.
- [67] L.M. Stapleton, A.N. Steele, H. Wang, H. Lopez Hernandez, A.C. Yu, M.J. Paulsen, A.A.A. Smith, G.A. Roth, A.D. Thakore, H.J. Lucian, K.P. Tothorow, S.W. Baker, Y. Tada, J.M. Farry, A. Eskandari, C.E. Hironaka, K.J. Jaatinen, K.M. Williams, H. Bergamasco, C. Marschel, B. Chadwick, F. Grady, M. Ma, E.A. Appel, Y.J. Woo, Use of a supramolecular polymeric hydrogel as an effective post-operative pericardial adhesion barrier, *Nat. Biomed. Eng.* 3 (2019) 611–620, doi:10.1038/s41551-019-0442-z.
- [68] A.M. Smith, J.A. Forder, S.R. Annareddy, K.S.K. Reddy, A.A. Amis, The porcine forelimb as a model for human flexor tendon surgery, *J. Hand Surg. Br.* 30 (2005) 307–309, doi:10.1016/j.jhsb.2005.02.003.
- [69] P.C. Amadio, Gliding Resistance and Modifications of Gliding Surface of Tendon: Clinical Perspectives, *Hand Clin* 29 (2013) 159–166, doi:10.1016/j.hcl.2013.02.001.
- [70] J.R. Fraser, B.J. Clarriss, E. Baxter, Patterns of induced variation in the morphology, hyaluronic acid secretion, and lysosomal enzyme activity of cultured human synovial cells, *Ann. Rheum. Dis.* 38 (1979) 287–294, doi:10.1136/ard.38.3.287.
- [71] H.I. Georgescu, D. Mendelow, C.H. Evans, HIG-82: An established cell line from rabbit periarticular soft tissue, which retains the "activatable" phenotype, *Vitr. Cell. Dev. Biol.* 24 (1988) 1015–1022, doi:10.1007/BF02620875.
- [72] S. Wan, S. Borland, S.M. Richardson, C.L.R. Merry, A. Saiani, J.E. Gough, Self-assembling peptide hydrogel for intervertebral disc tissue engineering, *Acta Biomater* 46 (2016) 29–40, doi:10.1016/j.actbio.2016.09.033.
- [73] A. Mujeeb, A.F. Miller, A. Saiani, J.E. Gough, Self-assembled octapeptide scaffolds for in vitro chondrocyte culture, *Acta Biomater* 9 (2013) 4609–4617, doi:10.1016/j.actbio.2012.08.044.
- [74] H. Yin, F. Strunz, Z. Yan, J. Lu, C. Brochhausen, S. Kiderlen, H. Clausen-Schaumann, X. Wang, M.E. Gomes, V. Alt, D. Docheva, Three-dimensional self-assembling nanofiber matrix rejuvenates aged/degenerative human tendon stem/progenitor cells, *Biomaterials* 236 (2020) 119802, doi:10.1016/j.biomaterials.2020.119802.
- [75] L.A. Castillo Diaz, M. Elsayy, A. Saiani, J.E. Gough, A.F. Miller, Osteogenic differentiation of human mesenchymal stem cells promotes mineralization within a biodegradable peptide hydrogel, *J. Tissue Eng* 7 (2016) 2041731416649789, doi:10.1177/2041731416649789.
- [76] M.D. Smith, The normal synovium, *Open Rheumatol. J.* 5 (2011) 100–106, doi:10.2174/1874312901105010100.